remote sensing

MDPI

Article

Remote Sensing of Local Warming Trend in Alberta, Canada during 2001–2020, and Its Relationship with Large-Scale Atmospheric Circulations

Quazi K. Hassan [1,*], Ifeanyi R. Ejiagha [1], M. Razu Ahmed [1], Anil Gupta [1,2], Elena Rangelova [1] and Ashraf Dewan [3]

[1] Department of Geomatics Engineering, Schulich School of Engineering, University of Calgary, 2500 University Dr. NW, Calgary, AB T2N 1N4, Canada; ifeanyi.ejiagha@ucalgary.ca (I.R.E.); mohammad.ahmed2@ucalgary.ca (M.R.A.); anil.gupta@gov.ab.ca (A.G.); evrangel@ucalgary.ca (E.R.)
[2] Resource Stewardship Division, Alberta Environment and Parks, 3535 Research Road NW, University Research Park, Calgary, AB T2L 2K8, Canada
[3] Spatial Sciences Discipline, School of Earth and Planetary Sciences, Curtin University, Kent Street, Bentley, WA 6102, Australia; A.Dewan@curtin.edu.au
* Correspondence: qhassan@ucalgary.ca; Tel.: +1-403-220-9494

Abstract: Here, the objective was to study the local warming trend and its driving factors in the natural subregions of Alberta using a remote-sensing approach. We applied the Mann–Kendall test and Sen's slope estimator on the day and nighttime MODIS LST time-series images to map and quantify the extent and magnitude of monthly and annual warming trends in the 21 natural subregions of Alberta. We also performed a correlation analysis of LST anomalies (both day and nighttime) of the subregions with the anomalies of the teleconnection patterns, i.e., Pacific North American (PNA), Pacific decadal oscillation (PDO), Arctic oscillation (AO), and sea surface temperature (SST, Niño 3.4 region) indices, to identify the relationship. May was the month that showed the most significant warming trends for both day and night during 2001–2020 in most of the subregions in the Rocky Mountains and Boreal Forest. Subregions of Grassland and Parkland in southern and southeastern parts of Alberta showed trends of cooling during daytime in July and August and a small magnitude of warming in June and August at night. We also found a significant cooling trend in November for both day and night. We identified from the correlation analysis that the PNA pattern had the most influence in the subregions during February to April and October to December for 2001–2020; however, none of the atmospheric oscillations showed any significant relationship with the significant warming/cooling months.

Keywords: Arctic oscillation (AO); Mann–Kendall test; Niño 3.4 region; Pacific decadal oscillation (PDO); Pacific North American (PNA) pattern; temperature anomaly

Citation: Hassan, Q.K.; Ejiagha, I.R.; Ahmed, M.R.; Gupta, A.; Rangelova, E.; Dewan, A. Remote Sensing of Local Warming Trend in Alberta, Canada during 2001–2020, and Its Relationship with Large-Scale Atmospheric Circulations. *Remote Sens.* **2021**, *13*, 3441. https://doi.org/10.3390/rs13173441

Academic Editor: Itamar Lensky

Received: 18 July 2021
Accepted: 25 August 2021
Published: 30 August 2021

1. Introduction

The world is continually experiencing warming (i.e., incremental rise in temperature over a long period of time) at an unprecedented rate [1]. This has been occurring over the decades as noticed from the steady increase in the global annual mean temperature anomaly [2]. Warming rates are nearly double in the northern high latitudes compared to the global average [3,4], Canada being the most impacted country [5]. It has been attributed to cumulative net CO_2 emissions, non-CO_2 radiative forcing agents (i.e., methane, aerosol, nitrous oxide, etc.), and anthropogenic activities such as industrialization and land-use/land-cover changes across the globe [6,7]. Warming at the global level has not been occurring at the same pattern at a local scale [8]. Incremental local temperature (i.e., local warming) has adverse effects on humans, natural resources, and the economic development of society. For instance, Quebec (an Eastern Canadian province) experienced high temperature that killed over 70 people in July 2018, while on the western coast of the

United States, the heatwave experienced in July 2017 caused constant forest fires within the surrounding western states that damaged about 609,509 acres of land and cost USD 92 million [9,10]. While attention has been paid to global- and regional-scale warming [11,12], studies on local warming are limited. Therefore, it is important to study warming at the local scale to comprehend its rate and pattern of occurrences to develop adaptation and mitigation strategies suitable for sustainable growth and development.

A common approach to quantify local warming is the use of weather-station-based temperature regimes over a long period [2,12]. This approach would be accurate if the quantity and quality of the temperature data are satisfactory. However, weather stations are sparsely distributed to produce continuous temperature dynamics over an area of interest. To address this issue, geographic information system (GIS)-based interpolation techniques can potentially be used. However, it provides different output maps with different techniques even when the same input station-based datasets are used [13–15]. Another alternative is to use remote-sensing-derived land surface temperature (LST) because of its repetitive coverage, synoptic view, and near-real-time data availability with global coverage [15,16].

Several studies can be found in the literature that used MODIS (moderate resolution imaging spectroradiometer)-acquired remote-sensing imagery for mapping warming trends. For example, Luintel et al. [17] and Yan et al. [9] used a time series of MODIS monthly LST at 5.6 km spatial resolution for mapping local warming trends of Nepal and North America, respectively, by applying linear regression analysis. Moreover, Rahaman and Hassan applied linear regression on an eight-day composite of MODIS LST at 1 km for the local warming trend in Alberta, Canada, and reported about 88.39% warming range of 0.75–1.0 °C in major cities and the Rocky Mountain areas [8]. Further, Olivares Contreras et al. [18] and Jiménez-Muñoz et al. [19] determined a warming rate of 0.78 and 0.33 °C/decade using the Mann–Kendall test and Sens's slope on time-series images of MODIS monthly LST over Patagonian Sub-Antarctic Forest, Chile (2001–2016), and Amazon Forest, Brazil (2000–2012), respectively. In addition, Aguilar-Lome et al. [20] and Qie et al. [21] applied the Mann–Kendall test and Sens's slope on the time series of MODIS 8-day (2000–2017) and daily (2001–2018) at 1 km for mapping the warming trends in South America (Peru, Bolivia, and Chile) and the Purog Kangri ice field, Qinghai–Tibetan Plateau, respectively. Overall, all these studies used the Mann–Kendall test, Sen's slope estimator, and linear regression techniques in determining local warming trends that are widely used in detecting trends of variables in meteorological and climate data for time-series studies [22–24]. In general, the non-parametric Mann–Kendall test is used in detecting trends, whereas Sen's slope indicates upward or downward trend (i.e., positive or negative slope, respectively) in a time series during the data period. Here, the Mann–Kendall test and Sen's slope have the advantage that they can be applied independent of the distribution pattern of the time series, while linear regression analysis can only be applied to normally distributed data. Though these studies succeeded in quantifying the local warming trend using remote-sensing imagery, they did not consider much in identifying the major driving factors of these anomalous changes in the local temperature.

Remote-sensing-based time-series trend analysis found that landscape characteristics and patterns such as land-use and land-cover changes, and therefore albedo changes, and elevation were responsible for anomalous changes in the local temperature. For example, Li et al. [25] monitored the spatiotemporal variation in LST of rural and urban regions of China from 2003 to 2013 and recorded an increasing temperature trend in urban regions, while Muster et al. [26] reported a high temperature variation in Arctic permafrost landscapes that was due to the changes in land cover and consequently surface albedo. Ejiagha et al. [27] also stated that composition and configuration of the urban landscape had influence on local warming. Meanwhile, Pepin et al. [28] showed that the local warming trend across the Tibetan Plateau depends on variations in the elevation. Additionally, studies showed that the influence of atmospheric, including aerosol, water vapour, and global circulations would be the major factors responsible for anomalous

temperature changes in the continental and local climate zones [9]. For example, sea surface temperature (SST) anomalies cause atmospheric changes that affect the climate of America [19,29]. Pacific, Atlantic, and Arctic Oceans surround the north of the continent, where complex climates significantly affect the natural environment; the glacial snow dominates the mountains in the west, where warming causes the melting of the glaciers [30]. The central part of the continent is constantly affected by air currents from the Arctic Ocean and the Gulf of Mexico due to the corridor formed by mountains in the east and west [9]. Greenland in the north is mainly covered by snow and ice that contributes to stabilizing the climate [31]. Therefore, marine bodies (i.e., Pacific, Atlantic, and Arctic Oceans) surrounding North America have a strong influence on their atmospheric changes and temperature anomalies that cause large-scale atmospheric circulations. For example, Pacific North American (PNA) patterns occur due to the alternating pressure patterns between the land and ocean (i.e., western North America including Western Canada and the Pacific Ocean, respectively) that push warmer temperature from the Pacific toward Canada from autumn to spring [32]. Pacific decadal oscillation (PDO) is the Pacific heating over a long period (20 to 30 years) that changes the pattern of SST anomalies in the North Pacific basin (20°N). El Niño–Southern Oscillation (ENSO), determined by the SST anomalies, is associated with winter temperature variations in Canada [33]. Here, El Niño is a warm phase when the anomaly equals or is more than 0.5 °C, and La Niña is a cold phase with an anomaly less than or equal to –0.5 °C. The positive phase of PDO causes warmer winter temperatures to occur in western and central Canada [34], whereas Arctic oscillation (AO) results due to the air pressure over the Arctic that becomes lower than the average. The positive phase of AO causes wind circulating around the North Pole to push colder air to the polar region during winter.

Yan et al. [9] analyzed the driving forces of North American LST anomalous changes considering the influence of vegetation, soil moisture, aerosol, atmospheric water vapour, SST, North Atlantic oscillation (NAO), and PDO. They reported an interannual and seasonal average warming rate of 0.02 °C/year and implied that the La Niña and El Niño events were the important drivers for the periodical lowest and highest LST, respectively. Though the study considered the influence of land surface and atmospheric parameters, it did not capture the monthly influence of these factors on the LST anomalous changes. In addition, local-scale analysis from the study on entire North America might not be appropriate to clearly understand the influence of these factors on the warming trend due to the aggregation of LST from different climate zones. Moreover, other parameters, such as AO and PNA patterns that would have a significant influence on North America, were not analyzed. The AO is the counterclockwise wind circulation around the Arctic that causes a shift in atmospheric pressure and temperature over time; the PNA pattern is the pressure fluctuations between the North Pacific Ocean and centers of action over western Canada and the southeastern United States [35]. Therefore, study of the correlations of LST changes with the atmospheric circulations and oscillations at the local scale is critical to understand the influential factors involved in local warming.

Landscape, topography, and climate characterize the natural (ecological) regions and subregions in an area. Therefore, it would be possible that anomalous changes of the local temperature (i.e., local warming) in the regions/subregions would be variable with a major influence of the atmospheric oscillations discussed in the previous paragraph. However, we did not find any literature, to the best of our knowledge, that determined and assessed the local warming at the natural subregional scale in the province of Alberta, Canada, considering the influence of the atmospheric factors. Although Rahaman and Hassan [8] showed the local warming trend in Alberta and its relationships with land use and land cover, they neither considered the influence of atmospheric circulations nor analyzed at the natural subregional level. On the other hand, Yan et al. determined the correlation coefficients of the atmospheric parameters with the mean LST anomaly considering entire North America as 71 grid units of 900 km $*$ 900 km (810,000 km^2). It would not be appropriate for the subregions of Alberta, where even Alberta (area of

661,848 km^2) itself is smaller than one grid they covered. Considering the limitations and issues identified from the literature, the overall objective was to comprehend the local warming trend and its driving factors in the natural subregions of Alberta using MODIS-acquired monthly LST data at 5.6 km spatial resolution. The specific objectives were: (i) quantification of monthly and annual warming trends in the 21 natural subregions of Alberta using the Mann–Kendall test and Sen's slope estimator on the day and nighttime MODIS LST time-series images; and (ii) correlation analysis of both day and nighttime LST anomalies of the 21 subregions with North American oscillations, i.e., SST anomaly, AO, PDO, and PNA patterns. Note that we excluded the NAO index from the analysis because it has a strong effect only on winter weather in Europe, Greenland, northeastern North America, North Africa, and Northern Asia [36], whereas Alberta is in the northwestern part of North America.

2. Study Area and Data Used

2.1. Description of the Study Area

We selected Alberta, a western Canadian province, as the study area (see Figure 1). It is between latitudes 49 and 60°N and longitudes 110 and 120°W with an area of 661,848 km^2. According to Statistics Canada, the population of Alberta increased from 2,974,807 in 2001 [37] to 4,067,175 in 2016 [38] and reached an estimated 4,436,258 as of 01 January, 2021 [39]. The major cities of Alberta are Calgary, Edmonton (Capital), Red Deer, and Lethbridge (see Figure 1), with a population of 1,361,852; 1,047,526; 106,736; and 101,324, respectively, as of 1st July 2020 [40]. The ecology of the area is geographically divided into six natural regions and 21 subregions (see Figure 1) based on the landscape patterns, vegetation, soil types, and physiographic features [41]. The distribution of these features is due to the combined influence of climate, topography, and geology in the area [42,43]. In terms of the climate of the study area, the mean temperature varies from −7.1 to 6 °C with long cold winters and short summers, and mean annual precipitation is 510 mm [41]. The elevation ranges from 150 to 3650 m above mean sea level [41].

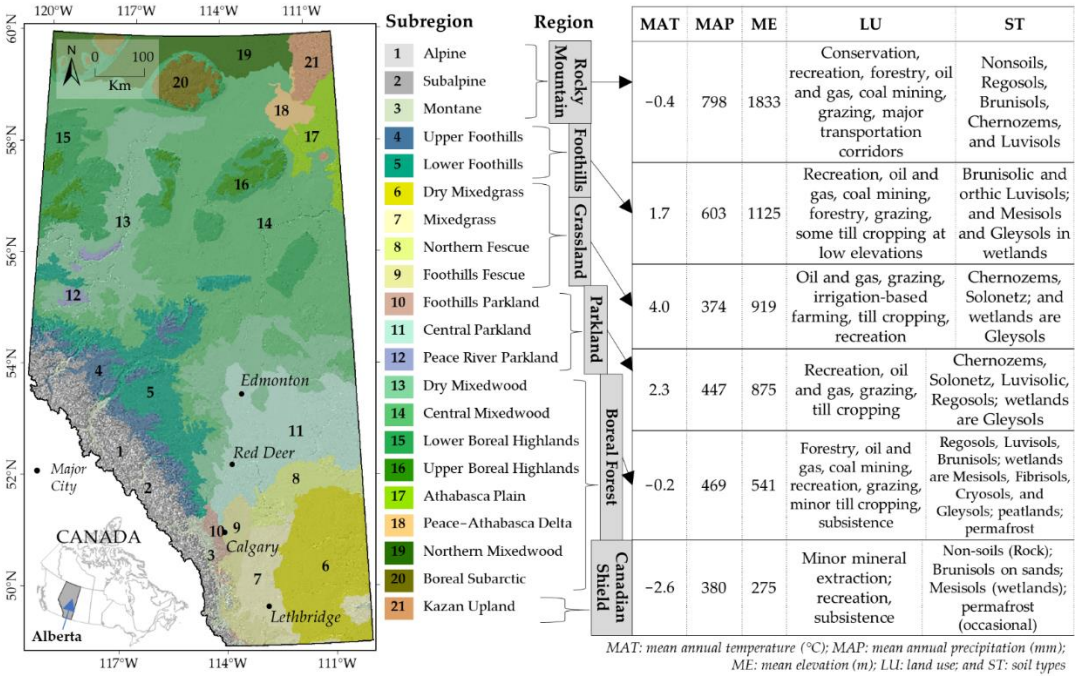

MAT	MAP	ME	LU	ST
−0.4	798	1833	Conservation, recreation, forestry, oil and gas, coal mining, grazing, major transportation corridors	Nonsoils, Regosols, Brunisols, Chernozems, and Luvisols
1.7	603	1125	Recreation, oil and gas, coal mining, forestry, grazing, some till cropping at low elevations	Brunisolic and orthic Luvisols; and Mesisols and Gleysols in wetlands
4.0	374	919	Oil and gas, grazing, irrigation-based farming, till cropping, recreation	Chernozems, Solonetz; and wetlands are Gleysols
2.3	447	875	Recreation, oil and gas, grazing, till cropping	Chernozems, Solonetz, Luvisolic, Regosols; wetlands are Gleysols
−0.2	469	541	Forestry, oil and gas, coal mining, recreation, grazing, minor till cropping, subsistence	Regosols, Luvisols, Brunisols; wetlands are Mesisols, Fibrisols, Cryosols, and Gleysols; peatlands; permafrost
−2.6	380	275	Minor mineral extraction; recreation, subsistence	Non-soils (Rock); Brunisols on sands; Mesisols (wetlands); permafrost (occasional)

Figure 1. Study area map showing the 21 natural subregions of Alberta and their characteristics.

2.2. Data Used and Their Preprocessing

We used three datasets in this study, including: (i) MODIS monthly LST image product (MOD11C3 Version 6) at 5.6 km for 2001–2020 acquired from the National Aeronautics and Space Administration (NASA); (ii) North American atmospheric oscillation indices, i.e., large-scale anomalies that influence the variability of the atmospheric circulations, from NOAA's National Centers for Environmental Information (NCEI); and (iii) shapefiles of the provincial boundary of Alberta and Alberta natural subregion obtained from geospatial data repository of the Government of Alberta. In the case of atmospheric oscillation indices, we used monthly tabular anomaly data of Niño 3.4 SST, AO, PDO, and PNA patterns for 2001–2020. We chose these four indices for their potential influences in the study area, including the following reasons: (i) the SST anomalies above and below the threshold of +0.5 °C and −0.5 °C cause El Niño and La Niña phenomena, respectively; (ii) the AO is characterized by winds circulating counter clockwise around the Arctic at around 55°N latitude; (iii) PDO is defined by the pattern of SST anomalies in the North Pacific basin of 20°N; and (iv) the positive phase of the PNA pattern is associated with above-average temperatures over western Canada and United States.

We preprocessed the acquired MODIS LST image in HDF formats to subset and mosaic for the study area in the NAD83 UTM Zone 12 North projection system. Next, we extracted layers of the LST and quality indicators for both day and nighttime. We used the quality layers to check for any low-quality pixels or gaps in the LST layers caused due to cloud or aerosol presence in the atmosphere during the image acquisition. The Bit flags in the quality indicator layer aided in interpreting the LST layers' quality assurance. We excluded those pixels where the average error for LST was greater than or equal to 3 K in the quality indicator layer. Note that such excluded pixels were negligible in the study area, i.e., 0.005 and 0.006% for day and nighttime images, respectively.

3. Methods

3.1. Mapping Local Warming Trend

We applied two non-parametric statistical tests, i.e., Mann–Kendall [44,45] and Sen's slope estimator [46], for determining the spatial and temporal (time-series) trends in the monthly and annual day and nighttime LST time series for both the entire study area (Alberta) and each of the 21 natural subregions. Moreover, we performed pixel-level trend analysis for mapping the spatial dynamics in the study area. We adopted these non-parametric statistical tests because they are independent of data distribution, insensitive to outliers, suitable for skewed data, and widely used for the trend analysis of atmospheric data [47,48].

3.1.1. Mann–Kendall Test

This test compared each value in the time series preceding it in sequential order, where the null hypothesis indicated no trend, and the alternative was a trend. To implement the statistical test, we calculated the sum of all the counts in the time series (i.e., statistics S) using Equation (1) [23].

$$S = \sum_{i=1}^{n-1} \sum_{j=i+1}^{n} sgn(x_j - x_i) \quad (1)$$

where the number of points is n, the values in the time series i and j are x_i and x_j, respectively (considering $j > i$), and the sign function is $sgn(x_j - x_i)$ calculated using Equation (2) [23].

$$sgn(x_j - x_i) = \begin{cases} +1 & if\ x_j - x_i > 0 \\ 0 & if\ x_j - x_i = 0 \\ -1 & if\ x_j - x_i < 0 \end{cases} \quad (2)$$

For large n, the S tends to normality with the variance, $var(\mathrm{S})$, calculated using Equation (3) [23].

$$var(\mathrm{S}) = \frac{1}{18}\left[n(n-1)(2n+5) - \sum_{i=1}^{m} t_i\ (t_i-1)(2t_i+5)\right] \quad (3)$$

where the length of time series and the number of tied values are n and m, respectively, and t_i is the number of ties of the extent i. Here, a tied value indicates a set of points with the same value.

Further, we used the standardized test statistics Z_S [49] to determine the nature of the trends in the time series (i.e., increasing and decreasing trends with positive and negative Z_S values, respectively) with the significance levels (p) at 90, 95, and 99% confidence (i.e., p equals to 0.10, 0.05, and 0.01, respectively). For the calculation of Z_S (considering $n > 10$), we used Equation (4) [23].

$$Z_S = \begin{cases} \frac{S-1}{\sqrt{var(S)}} & if\ S > 0 \\ 0 & if\ S = 0 \\ \frac{S+1}{\sqrt{var(S)}} & if\ S < 0 \end{cases} \quad (4)$$

3.1.2. Sen's Slope Estimator

We applied Sen's slope estimator (Q_i) to determine the magnitude of warming trend (i.e., slope) of each LST value in the time series for the N pairs of data using Equation (5) [23].

$$Q_i = \frac{x_j - x_k}{j-k} \quad for\ j = 1, 2, 3, \ldots, \ldots, \ldots, \ldots,\ N \quad (5)$$

where x_j and x_k are the values of data pairs at times j and k (considering $j > k$). Q_i ranks from the smallest to the largest, including the positive Q_i values for increasing or upward trends (warming), the negative values for decreasing or downward trends (cooling), and the zero values for no-trends (no change) in the LST values of the time series.

3.2. Correlating Atmospheric Oscillations

To determine the influence of North American atmospheric circulations in the study area and each of the 21 natural subregions, we performed a correlation analysis between anomalies of LST (monthly and annual for both day and nighttime) and the atmospheric oscillation indices (i.e., PNA, PDO, AO, and SST Niño 3.4). We calculated Pearson's correlation coefficient (r) using Equation (6) [50].

$$r = \left[\frac{\sum_{i=1}^{n}(x_i - \overline{x})(y_i - \overline{y})}{\sqrt{\sum_{i=1}^{n}(x_i - \overline{x})^2}\sqrt{\sum_{i=1}^{n}(y_i - \overline{y})^2}}\right] \quad (6)$$

where x_i and y_i are the values of x and y variables, respectively; $\overline{x}$ and $\overline{y}$ are the mean values of the x and y variables, respectively; and n is the number of observations.

4. Results

4.1. Analysis of Local Warming Trend at the Natural Subregion Scale

Monthly analysis revealed that May was having the most significant warming trends (0.15 to 0.32 °C/yr) in daytime LST for all the natural regions except Grassland, and two subregions from each of the Rocky Mountain (Subalpine and Montane) and Parkland (Foothills Parkland and Central Parkland) regions (see Table 1). In addition, we observed significant warming trends in June, August, and December for the Northern Mixedwood (0.08 °C/yr), Athabasca Plain (0.20 °C/yr), and Northern Fescue (0.01 °C/yr) subregions, respectively. All the warming trends were statistically significant at 95% confidence, except the Alpine subregion (90% confidence). Conversely, we found significant cooling trends for

the Grassland region in July (−0.14 to −0.34 °C/yr) and November (−0.31 to −0.36 °C/yr) except for Mixedgrass and Northern Fescue subregions, respectively. Furthermore, the Northern Fescue subregion showed a cooling trend in April. In the Parkland region, we noticed a significant cooling trend in July for the subregions of Foothills Parkland and Central Parkland, August for Central Parkland, and November for Peace River Parkland. Only one subregion (i.e., Dry Mixedwood) in the Boreal Forest region also showed a significant cooling trend in November. In the case of annual analysis, we did not find any significant warming trends, rather only cooling trends (−0.07 to −0.14 °C/yr) in the subregions of Montane (Rocky Mountains), Mixedgrass, Northern Fescue, and Foothills Fescue (Grassland), and Foothills Parkland and Central Parkland (Parkland).

In the case of monthly nighttime LST, we found a nearly similar pattern of warming trends with different magnitude (0.12 to 0.19 °C/yr) in May for all the natural regions, except Grassland and Canadian Shield, Montane subregion of the Rocky Mountain region, Foothills Parkland and Central Parkland in Parkland, and Athabasca Plain of Boreal Forest (see Table 2). In August, we observed it in Montane, Mixedgrass, Foothills Fescue, Foothills Parkland, Central Parkland, and Peace–Athabasca Delta subregions. In contrast, we noticed significant cooling trends in October for the Dry Mixedgrass and November for Dry Mixedgrass, Northern Fescue, and Northern Mixedwood subregions. However, we did not see any significant warming or cooling trends in the annual nighttimes. In general, we found warming trends occurred in the study area (Alberta) in May for both day and night at the rate of 0.14 and 0.11 °C/yr, respectively. From the linear regression model of the slopes of daytime and nighttime LSTs of subregions (see Figure 2), we discerned that they had an acceptable correlation (R^2 = 0.58), where the daytime is associated with an additional 0.60 of nighttime (i.e., nighttime was 60% cooler than the daytime).

The pixel-level spatial trend analysis revealed that daytime in May, June, July, August, November, and annual (see Table 3 and Figure 3a–f) and nighttime in May, June, August, and November (see Table 3 and Figure 3g–j) showed significant trends in at least 10% coverage of the study area with over 90% confidence levels. Among these, May was the significant month for the warming trends in both day and night with an area of 46.75 and 44.61%, respectively. This occurred in the 13 natural subregions in the northeastern, northern, northwestern, and western natural regions (Figure 3a,g), i.e., in most of Boreal Forest, Canadian Shield, Foothills, and the northern part of the Rocky Mountains. In the Rocky Mountain region (mostly Alpine and Subalpine subregions), area for the warming trend at night was more pronounced than for the day. In addition, we found areas of a significant warming trend in June and August with 7.90 and 7.43%, respectively, during the day scattered in the north and northeast (see Figure 3b,d), while it was 14.02 and 23.01%, respectively, at night scattered over the study area (see Figure 3h,i). We also found cooling trends of daytime during July, August, and November in the eastern, southeastern, and southern parts of the study area mostly in the Grassland and Parkland regions (see Figure 3c–e) and some areas in the centre and west under the Foothills and Boreal Forest regions in November (see Figure 3e). The nighttime cooling trend in November showed the spatial distribution scattered from the northwest to southeast through the centre in the study area (see Figure 3j).

Table 1. Daytime LST trend (°C/yr) during 2001–2020 (monthly and annual) for the 21 natural subregions in Alberta using Mann–Kendall test. The significant values are highlighted italic, where ^, *, and ** indicate the 90, 95, and 99% confidence levels, respectively.

Natural Region	Natural Subregion	Month												Annual
		Jan	Feb	Mar	Apr	May	Jun	Jul	Aug	Sep	Oct	Nov	Dec	
Rocky Mountain	Alpine	−0.018	−0.162	0.020	−0.025	*0.163* ^	−0.025	−0.023	0.011	0.047	−0.047	−0.009	0.036	−0.008
	Subalpine	−0.005	−0.163	−0.008	−0.020	0.162	−0.046	−0.020	0.035	0.024	−0.067	−0.048	0.038	−0.018
	Montane	−0.074	−0.107	−0.199	−0.111	0.054	−0.064	−0.081	0.028	−0.012	−0.130	−0.192	0.033	*−0.066* *
Foothills	Upper Foothills	−0.020	−0.222	−0.044	−0.062	*0.166* *	−0.023	−0.038	0.029	0.045	−0.049	−0.185	0.070	−0.023
	Lower Foothills	−0.010	−0.172	−0.020	−0.129	*0.189* *	−0.031	−0.060	−0.010	0.044	0.008	−0.260	0.113	−0.037
Grassland	Dry Mixedgrass	−0.081	−0.119	−0.023	−0.271	0.045	0.046	*−0.226* ^	0.050	0.025	−0.127	*−0.311* ^	−0.007	−0.088
	Mixedgrass	−0.085	−0.173	−0.084	−0.186	0.027	−0.040	−0.190	0.061	0.092	−0.179	*−0.344* ^	−0.003	*−0.111* ^
	Northern Fescue	−0.043	−0.094	−0.007	*−0.308* *	0.007	−0.064	*−0.341* *	−0.157	−0.082	−0.046	−0.310	*0.007* *	*−0.142* **
	Foothills Fescue	−0.085	−0.130	−0.128	−0.167	0.090	−0.057	*−0.142* **	0.020	0.031	−0.149	*−0.360* *	−0.065	*−0.120* *
Parkland	Foothills Parkland	−0.183	−0.122	−0.143	−0.066	0.089	−0.046	*−0.108* ^	−0.009	−0.013	−0.146	−0.258	−0.017	*−0.093* ^
	Central Parkland	−0.004	−0.108	0.030	−0.246	0.003	−0.066	*−0.198* *	*−0.204* *	−0.077	−0.044	−0.278	0.034	*−0.126* *
	Peace River Parkland	0.059	−0.015	0.001	−0.037	*0.245* *	−0.117	−0.126	−0.097	0.008	−0.012	*−0.368* *	0.186	−0.023
Boreal Forest	Dry Mixedwood	0.068	−0.092	−0.016	−0.153	*0.163* *	−0.025	−0.128	−0.038	−0.011	−0.058	*−0.273* ^	0.151	−0.052
	Central Mixedwood	0.056	−0.147	0.044	−0.117	*0.154* *	0.024	−0.046	0.051	0.001	−0.109	−0.202	0.052	0.001
	Lower Boreal Highlands	0.017	−0.203	0.058	−0.138	*0.214* *	0.010	−0.019	0.043	−0.084	−0.068	−0.154	0.047	0.005
	Upper Boreal Highlands	0.099	−0.133	0.031	−0.087	*0.189* *	0.024	0.007	0.064	0.019	−0.112	−0.230	0.015	0.000
	Athabasca Plain	0.029	−0.208	−0.009	0.035	*0.320* *	0.108	0.030	*0.199* *	−0.032	−0.155	−0.219	−0.134	−0.006
	Peace–Athabasca Delta	0.003	−0.128	0.037	0.051	*0.240* *	0.000	−0.026	0.107	0.000	−0.170	−0.212	−0.123	−0.017
	Northern Mixedwood	0.028	−0.162	0.057	−0.013	*0.248* *	*0.080* *	0.039	0.106	0.014	−0.097	−0.128	−0.004	0.026
	Boreal Subarctic	0.109	−0.154	0.052	0.046	*0.225* *	0.036	−0.035	0.051	0.043	−0.086	−0.103	−0.032	0.022
Canadian Shield	Kazan Upland	0.011	−0.097	−0.017	−0.016	*0.230* *	−0.015	−0.005	0.116	−0.024	−0.185	−0.110	−0.029	−0.013
Alberta (Study area)		−0.026	−0.127	0.038	−0.131	*0.141* *	0.004	−0.079	0.002	−0.004	−0.047	−0.219	0.044	−0.032

Table 2. Nighttime LST trend (°C/yr) during 2001–2020 (monthly and annual) for the 21 natural subregions in Alberta using Mann–Kendall test. The significant values are highlighted italic, where ^, *, and ** indicate the 90, 95, and 99% confidence levels, respectively.

Natural Region	Natural Subregion	Month												Annual
		Jan	Feb	Mar	Apr	May	Jun	Jul	Aug	Sep	Oct	Nov	Dec	
Rocky Mountain	Alpine	0.053	−0.117	0.027	−0.013	*0.190* *	0.019	0.013	0.060	0.013	−0.050	−0.023	−0.003	0.013
	Subalpine	0.029	−0.120	0.019	−0.003	*0.172* *	−0.008	−0.013	0.085	0.023	−0.049	−0.026	−0.011	0.008
	Montane	0.022	−0.072	−0.104	−0.067	0.049	0.042	−0.044	*0.095* ^	0.020	−0.047	−0.103	0.056	0.002
Foothills	Upper Foothills	−0.022	−0.255	−0.064	−0.074	*0.136* *	0.027	−0.017	0.059	0.030	−0.075	−0.139	0.047	−0.027
	Lower Foothills	0.018	−0.211	−0.045	−0.097	*0.118* *	0.033	−0.004	0.056	0.006	−0.070	−0.193	0.023	−0.021
Grassland	Dry Mixedgrass	−0.089	−0.050	−0.134	−0.136	−0.013	0.027	−0.058	0.075	0.007	*−0.150* ^	*−0.188* *	−0.005	−0.041
	Mixedgrass	−0.024	−0.073	−0.140	−0.075	0.000	0.042	−0.038	*0.089* ^	0.026	−0.108	−0.102	0.032	−0.017
	Northern Fescue	0.037	−0.155	−0.069	−0.143	0.014	0.030	−0.014	0.063	−0.007	−0.074	*−0.252* ^	0.013	−0.056
	Foothills Fescue	−0.018	−0.124	−0.124	−0.095	−0.007	0.034	−0.032	*0.082* *	0.043	−0.092	−0.105	0.074	−0.022
Parkland	Foothills Parkland	−0.029	−0.118	−0.094	−0.091	0.010	0.051	−0.019	*0.091* *	0.062	−0.070	−0.100	0.034	−0.020
	Central Parkland	0.042	−0.176	−0.022	−0.107	0.093	0.073	0.007	*0.071* *	0.053	−0.052	−0.253	0.098	−0.040
	Peace River Parkland	0.032	−0.130	−0.053	−0.031	*0.182* *	0.018	−0.022	0.078	0.026	−0.084	−0.197	0.037	−0.007
Boreal Forest	Dry Mixedwood	0.007	−0.232	−0.007	−0.145	*0.149* *	0.051	−0.001	0.060	−0.040	−0.082	−0.200	0.107	−0.041
	Central Mixedwood	0.062	−0.053	0.045	−0.111	*0.139* ^	0.038	0.012	0.105	0.039	−0.065	−0.210	0.040	−0.021
	Lower Boreal Highlands	0.125	−0.098	0.049	−0.072	*0.188* **	0.031	0.018	0.099	0.034	−0.079	−0.244	0.078	−0.013
	Upper Boreal Highlands	0.109	−0.085	0.004	−0.060	*0.186* *	0.053	0.021	0.079	0.036	−0.077	−0.244	0.049	−0.012
	Athabasca Plain	−0.006	−0.108	0.001	−0.109	0.151	0.069	0.016	0.059	0.049	−0.097	−0.189	−0.113	−0.031
	Peace–Athabasca Delta	0.088	−0.082	0.009	−0.086	*0.164* ^	0.094	0.033	*0.137* ^	0.075	−0.101	−0.199	−0.089	0.001
	Northern Mixedwood	0.058	−0.101	0.043	−0.123	*0.134* *	0.038	−0.022	0.119	0.030	−0.064	*−0.200* ^	0.047	−0.009
	Boreal Subarctic	0.095	−0.089	0.106	−0.100	*0.157* *	0.040	−0.014	0.095	0.036	−0.034	−0.219	0.058	−0.002
Canadian Shield	Kazan Upland	0.057	−0.099	−0.007	−0.116	0.149	0.052	−0.001	0.063	0.001	−0.137	−0.151	−0.086	−0.026
Alberta (Study area)		0.010	−0.097	−0.020	−0.087	*0.114* ^	0.050	−0.002	0.085	0.031	−0.085	−0.197	0.039	−0.028

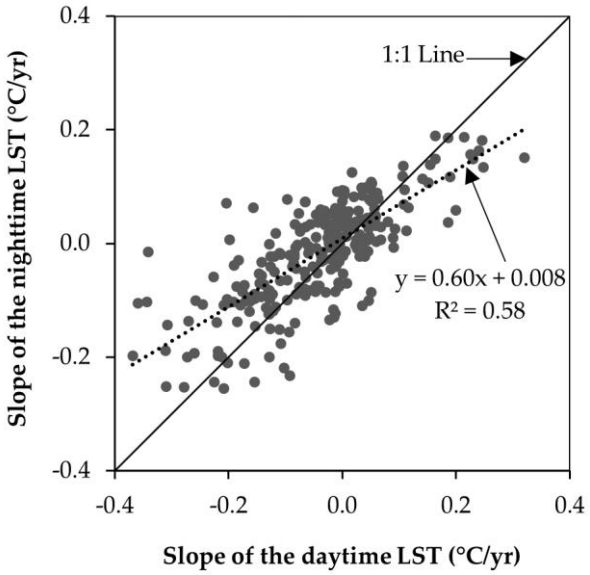

Figure 2. Comparison of Sen's slope for the daytime and nighttime LST.

Table 3. Area coverage in percentage warming and cooling trends for over 90% confidence levels.

LST	Confidence Level (%)		Area Coverage (%)												
			Jan	**Feb**	**Mar**	**Apr**	**May**	**Jun**	**Jul**	**Aug**	**Sep**	**Oct**	**Nov**	**Dec**	**Annual**
Day	Not significant		98.72	97.24	99.71	94.15	53.21	87.62	77.13	83.09	99.90	97.77	76.59	99.98	78.98
	Cooling	≥90	0.21	2.19	0.22	4.08	0.04	2.57	8.65	2.95	0.07	1.78	16.86	0.01	7.61
		≥95	0.02	0.56	0.04	1.71	0.00	1.59	10.20	4.31	0.01	0.43	6.44	0.00	10.12
		≥99	0.00	0.01	0.00	0.06	0.00	0.33	2.38	2.21	0.00	0.01	0.11	0.00	2.81
	Warming	≥90	0.80	0.00	0.03	0.00	15.26	3.05	0.90	3.56	0.02	0.00	0.00	0.01	0.29
		≥95	0.25	0.00	0.00	0.00	23.15	3.76	0.69	3.21	0.00	0.00	0.00	0.00	0.19
		≥99	0.00	0.00	0.00	0.00	8.34	1.09	0.06	0.66	0.00	0.00	0.00	0.00	0.00
Night	Not significant		99.34	97.01	99.58	94.61	55.37	85.48	97.61	76.98	99.71	97.15	78.88	99.94	96.17
	Cooling	≥90	0.10	2.28	0.33	4.44	0.03	0.29	1.19	0.00	0.00	2.12	15.07	0.00	2.36
		≥95	0.03	0.67	0.03	0.93	0.00	0.16	0.40	0.00	0.00	0.72	5.88	0.00	1.12
		≥99	0.00	0.03	0.00	0.00	0.00	0.04	0.02	0.00	0.00	0.00	0.17	0.00	0.22
	Warming	≥90	0.47	0.00	0.06	0.02	14.00	7.40	0.52	13.29	0.23	0.00	0.00	0.06	0.11
		≥95	0.06	0.00	0.00	0.00	21.88	5.46	0.23	8.67	0.05	0.00	0.00	0.00	0.01
		≥99	0.00	0.00	0.00	0.00	8.73	1.16	0.04	1.05	0.00	0.00	0.00	0.00	0.00

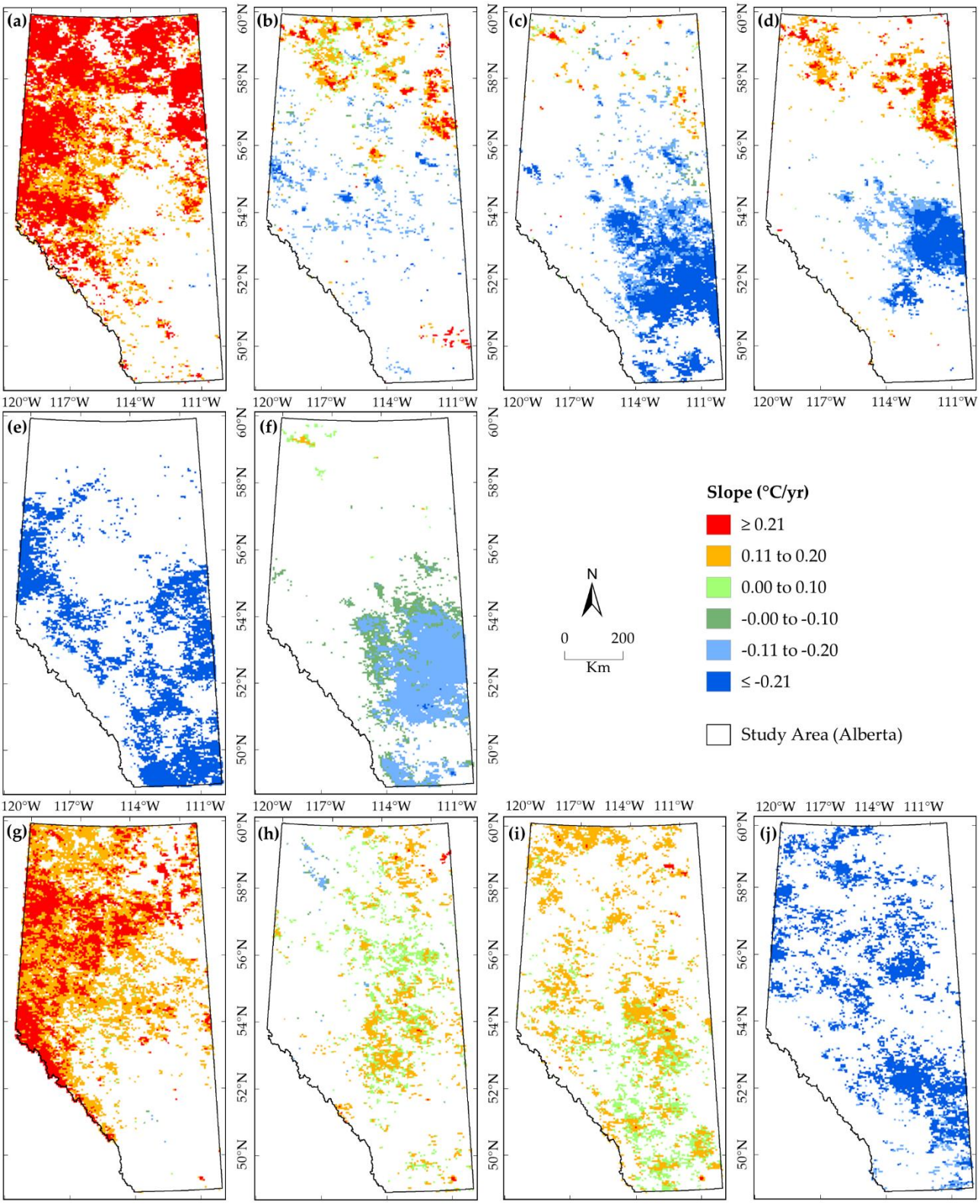

Figure 3. Spatial pattern of day and nighttime LST warming and cooling trends over 90% confidence levels. Daytime months are May (**a**), June (**b**), July (**c**), August (**d**), November (**e**), and annual (**f**); nighttime months are May (**g**), June (**h**), August (**i**), and November (**j**), where they showed trends in at least 10% area in Alberta.

4.2. Correlation Analysis of LST Anomalies with the Atmospheric Oscillations

We presented the correlations of the day and nighttime LST anomalies in the natural subregions with the PNA, PDO, AO, and SST (Niño 3.4) patterns in Tables 4–7, respectively. The PNA pattern showed acceptable to very good positive correlations (r = 0.50 to 0.89) in February, March, April, October, November, and December in all subregions and entire Alberta for both day and night, with very few exceptions. Here, we used a classification scheme to assess the performance of the Pearson correlation analysis, i.e., unsatisfactory ($r \leq 0.4$), acceptable (r = 0.40–0.60), satisfactory (r = 0.60–0.70), good (r = 0.70–0.85), and very good (r = 0.85–1.00) [51,52]. The exceptions for daytime were in four subregions in February (Athabasca Plain, Peace–Athabasca Delta, Northern Mixedwood, and Kazan Upland), one in March (Northern Fescue), one in October (Foothills Fescue), and two in November (Lower Boreal Highlands and Kazan Upland); and one each in April (Boreal Subarctic) and December (Montane) for nighttime (see Table 4). We also found acceptable and satisfactory positive correlations (r = 0.51 to 0.62) in January for the subregions of Alpine, Subalpine, Upper Foothills, Lower Foothills, and Dry Mixedwood during the day and Alpine and Subalpine during the night (see Table 4).

In the case of the PDO, we observed acceptable to good positive correlations with the LST anomalies (r = 0.52 to 0.74) in all eight natural subregions of the Rocky Mountains, Foothills, and Parkland regions during both the day and night in April, including the entire Alberta (see Table 5). In April, all subregions of Grassland showed acceptable to good positive correlation during night, where some subregions of Boreal Forest showed acceptable during the day or night. We also found above the acceptable positive correlations in the Alpine and Subalpine subregions for January and Alpine and Northern Mixedwood for annual during the day and night, in addition to Foothills Fescue for March during the day and Lower Boreal Highlands for April during the night (see Table 5).

We noticed the acceptable to good correlations between the LST anomalies of the subregions and AO index were negative in April (r = −0.51 to −0.74) and positive in June (r = 0.50 to 0.77) (see Table 6). The negative correlations were in the Rocky Mountain, Foothills (except Lower Foothills at night), Grassland (except Dry Mixedgrass and Northern Fescue during the day), and Parkland (except Peace River Parkland during the day and night and Central Parkland at night) regions during both the day and night. In contrast, we observed positive correlations in June during the night for all subregions with the exception of Alpine, Subalpine, Peace–Athabasca Delta, and Kazan Upland, while during the day for the Alpine, Subalpine, Upper Foothills, Central Mixedwood, Lower Boreal Highlands, Upper Boreal Highlands, Peace–Athabasca Delta, Boreal Subarctic, and Kazan Upland subregions (see Table 6). In addition, we found positive correlations during nights in August for Peace River Parkland and Boreal Subarctic and during days in October for Lower Boreal Highlands and Peace–Athabasca Delta subregions. The correlations of the entire Alberta were negative (r = −0.51) during the day in April and good positive (r = 0.77) at night in June (see Table 6).

In most of the cases, the correlation between the LST anomalies and Niño 3.4 SST indicated a weak relationship, except in April with five subregions (Alpine, Subalpine, Montane, Upper Foothills, and Foothills Parkland) for the day and two (Alpine and Subalpine) for the night, June with four subregions (Dry Mixedgrass, Mixedgrass, Northern Fescue, and Dry Mixedwood) for the day, and July with one subregion (Northern Fescue) for the day (see Table 7). In addition, the entire Alberta showed an acceptable positive correlation (r = 0.57) in June during the day.

Table 4. Relations between day and nighttime LST and PNA indices at both monthly and annual timescales, where acceptable correlations ($r \geq 0.50$) are highlighted italic.

Month	Natural Region	Rocky Mountain			Foothills			Grassland			Parkland							Boreal Forest					Ca Sd	Alberta
	Subregion	1	2	3	4	5	6	7	8	9	10	11	12	13	14	15	16	17	18	19	20	21		
Jan	Day	*0.62*	*0.57*	0.30	*0.52*	*0.51*	0.11	0.00	0.25	0.02	0.21	0.39	0.49	*0.51*	0.41	0.48	0.43	0.27	0.24	0.46	0.43	0.35	0.44	
	Night	*0.61*	*0.61*	0.29	0.42	0.46	0.34	0.30	0.46	0.30	0.31	0.44	0.43	0.47	0.45	0.47	0.44	0.33	0.29	0.42	0.42	0.42	0.48	
Feb	Day	*0.82*	*0.82*	*0.78*	*0.80*	*0.77*	*0.66*	*0.72*	*0.67*	*0.75*	*0.79*	*0.70*	*0.71*	*0.70*	*0.59*	*0.60*	*0.66*	0.40	0.37	0.46	*0.59*	0.32	*0.71*	
	Night	*0.82*	*0.81*	*0.71*	*0.80*	*0.78*	*0.62*	*0.68*	*0.66*	*0.66*	*0.71*	*0.70*	*0.81*	*0.70*	*0.65*	*0.69*	*0.67*	*0.50*	*0.51*	*0.57*	*0.63*	*0.51*	*0.73*	
Mar	Day	*0.56*	*0.59*	*0.58*	*0.60*	*0.60*	*0.51*	*0.56*	0.49	*0.55*	*0.57*	*0.52*	*0.64*	*0.63*	*0.63*	*0.64*	*0.63*	*0.66*	*0.63*	*0.58*	*0.60*	*0.62*	*0.64*	
	Night	*0.61*	*0.61*	*0.52*	*0.60*	*0.58*	*0.49*	*0.51*	*0.53*	*0.53*	*0.51*	*0.55*	*0.59*	*0.61*	*0.62*	*0.63*	*0.63*	*0.60*	*0.58*	*0.65*	*0.59*	*0.58*	*0.63*	
Apr	Day	*0.73*	*0.73*	*0.75*	*0.80*	*0.81*	*0.53*	*0.59*	*0.64*	*0.65*	*0.68*	*0.75*	*0.69*	*0.76*	*0.78*	*0.76*	*0.79*	*0.66*	*0.63*	*0.72*	*0.75*	*0.68*	*0.79*	
	Night	*0.72*	*0.72*	*0.75*	*0.80*	*0.78*	*0.68*	*0.74*	*0.75*	*0.78*	*0.83*	*0.72*	*0.70*	*0.68*	*0.74*	*0.77*	*0.77*	*0.67*	*0.64*	*0.72*	0.14	*0.66*	*0.79*	
May	Day	0.08	0.07	0.03	0.15	0.03	−0.17	−0.13	−0.19	−0.10	−0.08	−0.31	0.00	−0.06	0.03	0.13	0.13	0.09	0.04	0.21	0.22	0.09	0.01	
	Night	0.20	0.17	−0.01	0.19	0.22	−0.24	−0.23	−0.22	−0.12	0.07	−0.01	0.38	0.20	0.12	0.17	0.14	0.13	0.07	0.14	0.12	0.11	0.11	
Jun	Day	−0.09	−0.11	0.09	−0.04	−0.11	0.23	0.15	0.17	0.14	0.17	0.15	−0.04	0.02	−0.05	0.07	−0.15	−0.06	−0.26	−0.07	0.06	−0.34	0.05	
	Night	−0.04	−0.06	0.14	−0.09	−0.08	0.14	0.13	0.01	0.04	0.16	0.04	0.06	−0.01	−0.25	−0.27	−0.29	−0.42	−0.39	−0.36	−0.30	−0.43	−0.15	
Jul	Day	0.38	0.39	0.37	0.30	0.29	0.24	0.21	0.21	0.23	0.25	0.20	0.32	0.28	0.12	0.08	0.08	−0.22	−0.30	−0.25	−0.22	−0.20	0.23	
	Night	0.29	0.31	0.36	0.29	0.29	0.37	0.42	0.42	0.44	0.35	0.36	0.13	0.20	0.16	0.06	0.09	−0.10	−0.12	−0.20	−0.02	−0.15	0.23	
Aug	Day	−0.15	−0.13	−0.13	−0.13	−0.24	−0.22	−0.21	−0.22	−0.24	−0.15	−0.33	−0.24	−0.38	−0.37	−0.23	−0.24	−0.30	−0.51	−0.34	−0.21	−0.43	−0.34	
	Night	−0.17	−0.17	−0.01	−0.14	−0.24	−0.13	−0.03	−0.32	−0.04	−0.09	−0.35	−0.23	−0.30	−0.31	−0.29	−0.29	−0.42	−0.30	−0.42	−0.35	−0.43	−0.30	
Sep	Day	−0.32	−0.32	−0.35	−0.31	−0.35	−0.30	−0.32	−0.32	−0.29	−0.33	−0.28	−0.26	−0.33	−0.39	−0.19	−0.41	−0.53	−0.55	−0.43	−0.35	−0.48	−0.37	
	Night	−0.30	−0.32	−0.35	−0.28	−0.29	−0.21	−0.22	−0.28	−0.21	−0.24	−0.25	−0.24	−0.10	−0.35	−0.37	−0.38	−0.38	−0.34	−0.40	−0.42	−0.41	−0.33	
Oct	Day	*0.52*	*0.54*	*0.57*	*0.59*	*0.56*	*0.52*	*0.52*	*0.54*	0.49	*0.57*	*0.62*	*0.57*	*0.60*	*0.60*	*0.55*	*0.60*	*0.52*	*0.50*	*0.54*	*0.52*	*0.56*	*0.60*	
	Night	*0.55*	*0.58*	*0.53*	*0.62*	*0.67*	*0.61*	*0.60*	*0.65*	*0.53*	*0.51*	*0.65*	*0.63*	*0.68*	*0.62*	*0.62*	*0.64*	*0.58*	*0.53*	*0.57*	*0.62*	*0.57*	*0.65*	
Nov	Day	*0.68*	*0.69*	*0.59*	*0.66*	*0.65*	*0.63*	*0.51*	*0.67*	*0.59*	*0.60*	*0.70*	*0.51*	*0.62*	*0.55*	0.46	*0.56*	*0.50*	*0.53*	*0.54*	*0.56*	0.42	*0.64*	
	Night	*0.58*	*0.62*	*0.67*	*0.63*	*0.61*	*0.70*	*0.61*	*0.74*	*0.64*	*0.67*	*0.71*	*0.59*	*0.55*	*0.56*	*0.56*	*0.55*	*0.53*	*0.56*	*0.60*	*0.58*	*0.54*	*0.64*	
Dec	Day	*0.63*	*0.66*	*0.67*	*0.78*	*0.82*	*0.74*	*0.71*	*0.75*	*0.71*	*0.71*	*0.73*	*0.70*	*0.79*	*0.84*	*0.88*	*0.89*	*0.79*	*0.78*	*0.86*	*0.87*	*0.75*	*0.84*	
	Night	*0.56*	*0.58*	0.38	*0.76*	*0.75*	*0.62*	*0.53*	*0.75*	*0.51*	*0.53*	*0.70*	*0.61*	*0.76*	*0.85*	*0.87*	*0.88*	*0.80*	*0.80*	*0.82*	*0.79*	*0.75*	*0.83*	
Annual	Day	0.10	0.11	0.20	0.21	0.14	0.08	0.23	0.12	0.13	0.17	0.21	0.17	0.08	0.23	0.08	0.19	0.15	0.11	0.13	0.20	0.10	0.18	
	Night	0.13	0.21	0.17	0.21	0.21	0.11	0.21	0.19	0.22	0.18	0.23	0.11	0.13	0.12	0.25	0.25	0.24	0.08	0.10	0.24	0.12	0.21	

Region: **Ca Sd:** Canadian Shield; Subregion: **1.** Alpine; **2.** Alpine; **3:** Montane; **4:** Upper Foothills; **5:** Lower Foothills; **6:** Dry Mixedgrass; **7:** Mixedgrass; **8:** Northern Fescue; **9:** Foothills Fescue; **10:** Foothills Parkland; **11:** Central Parkland; **12:** Peace River Parkland; **13:** Dry Mixedwood; **14:** Central Mixedwood; **15:** Upper Boreal Highlands; **17:** Athabasca Plain; **18:** Peace–Athabasca Delta; **19:** Northern Mixedwood; **20:** Boreal Subarctic; **21:** Kazan Upland.

Table 5. Relations between day and nighttime LST and PDO indices at both monthly and annual timescales, where acceptable correlations ($r \geq 0.50$) are highlighted italic.

Month	Natural Region	Rocky Mountain			Foothills			Grassland			Parkland							Boreal Forest					Ca Sd	Alberta
	Subregion	1	2	3	4	5	6	7	8	9	10	11	12	13	14	15	16	17	18	19	20	21	
Jan	Day	*0.57*	*0.58*	0.46	0.45	0.15	0.08	0.15	0.14	0.21	0.40	0.20	0.04	0.16	0.16	0.17	0.24	0.14	0.19	0.30	0.33	0.23	0.23
	Night	*0.69*	*0.68*	0.44	0.44	0.32	0.25	0.33	0.32	0.32	0.42	0.32	0.20	0.29	0.35	0.32	0.33	0.48	0.41	0.43	0.44	0.53	0.40
Feb	Day	0.22	0.20	0.20	0.15	0.16	0.09	0.17	0.07	0.21	0.21	0.10	0.14	0.12	−0.04	0.00	0.03	−0.26	−0.22	−0.11	−0.11	−0.27	0.06
	Night	0.26	0.24	0.18	0.14	0.11	0.04	0.13	0.10	0.14	0.14	0.11	0.19	0.11	0.05	0.11	0.07	−0.11	−0.05	0.01	−0.02	−0.11	0.10
Mar	Day	0.39	0.44	0.49	0.44	0.42	0.47	0.47	0.45	*0.50*	0.45	0.44	0.45	0.44	0.40	0.48	0.44	0.30	0.26	0.42	0.47	0.33	0.47
	Night	0.40	0.41	0.32	0.39	0.40	0.34	0.27	0.44	0.31	0.31	0.46	0.43	0.43	0.40	0.43	0.40	0.29	0.30	0.42	0.46	0.29	0.43
Apr	Day	*0.70*	*0.69*	*0.65*	*0.69*	*0.63*	0.38	0.44	0.36	0.44	*0.67*	*0.52*	*0.55*	*0.59*	*0.55*	*0.51*	*0.52*	0.39	0.35	0.48	0.49	0.38	*0.59*
	Night	*0.73*	*0.74*	*0.63*	*0.68*	*0.64*	*0.60*	*0.66*	*0.60*	*0.67*	*0.62*	*0.60*	*0.55*	0.45	0.45	*0.51*	0.48	0.26	0.26	0.36	0.34	0.24	*0.56*
May	Day	0.40	0.38	0.12	0.23	0.28	0.20	0.23	0.22	0.24	0.18	0.28	0.39	0.30	0.17	0.28	0.18	0.11	0.08	0.22	0.20	0.11	0.27
	Night	0.18	0.20	0.18	0.11	−0.01	0.00	0.07	0.06	0.06	0.04	0.11	0.04	0.07	0.01	0.08	0.08	0.01	0.15	0.04	0.14	−0.01	0.06
Jun	Day	0.44	0.43	0.20	0.35	0.22	0.25	0.26	0.06	0.19	0.24	−0.04	0.01	0.05	0.16	0.38	0.30	−0.10	−0.06	0.32	0.29	−0.13	0.22
	Night	0.45	0.45	0.47	0.38	0.41	0.26	0.36	0.16	0.37	0.45	0.29	0.58	0.47	0.29	0.27	0.20	−0.04	−0.03	−0.15	−0.05	−0.16	0.36
Jul	Day	0.19	0.20	0.25	0.22	0.22	0.31	0.21	0.20	0.14	0.24	0.14	0.08	0.24	0.18	0.20	0.12	−0.25	−0.23	0.01	0.00	−0.14	0.23
	Night	0.23	0.26	0.29	0.26	0.26	0.17	0.26	0.14	0.33	0.38	0.10	0.10	0.16	0.14	0.09	0.08	−0.15	−0.23	−0.14	−0.05	−0.42	0.16
Aug	Day	0.10	0.05	0.04	−0.11	−0.04	−0.05	0.04	0.10	0.06	0.04	0.15	−0.09	−0.03	−0.17	−0.22	−0.28	−0.24	−0.23	−0.22	−0.21	−0.17	−0.08
	Night	0.14	0.06	−0.09	−0.16	−0.25	−0.02	−0.03	−0.11	−0.05	−0.03	−0.21	−0.38	−0.37	−0.37	−0.38	−0.40	−0.36	−0.31	−0.36	−0.41	−0.33	−14.40
Sep	Day	−0.25	−0.24	−0.19	−0.18	0.07	−0.13	−0.09	−0.15	−0.11	−0.13	−0.12	−0.16	−0.17	−0.22	−0.29	−0.19	−0.17	−0.13	−0.10	−0.16	−0.14	−0.18
	Night	−0.23	−0.20	−0.10	−0.19	−0.19	−0.06	0.00	−0.10	−0.05	−0.10	−0.08	−0.13	−0.25	−0.20	−0.19	−0.17	−0.18	−0.17	−0.27	−0.31	−0.18	−0.18
Oct	Day	0.26	0.25	0.15	0.23	0.22	0.17	0.18	0.22	0.18	0.16	0.27	0.20	0.17	0.12	0.09	0.05	−0.06	−0.05	0.03	0.06	−0.12	0.16
	Night	0.27	0.27	0.14	0.18	0.12	0.10	0.09	0.15	0.12	0.10	0.12	0.09	0.05	−0.04	−0.03	0.00	−0.17	−0.17	−0.09	0.01	−0.21	0.04
Nov	Day	0.30	0.25	−0.15	−0.02	−0.07	−0.21	−0.32	−0.16	−0.24	−0.24	−0.08	−0.08	−0.04	0.00	0.06	−0.01	0.04	0.03	0.19	0.17	0.04	−0.03
	Night	0.20	0.21	0.11	−0.05	−0.11	0.11	0.04	0.21	0.07	0.03	0.05	−0.02	−0.01	−0.03	−0.01	−0.03	0.02	0.06	0.11	0.10	0.02	0.02
Dec	Day	0.20	0.21	0.15	0.28	0.26	0.38	0.30	0.39	0.28	0.24	0.32	0.29	0.28	0.26	0.31	0.37	0.24	0.22	0.30	0.36	0.18	0.30
	Night	0.17	0.18	0.00	0.32	0.35	0.19	0.14	0.36	0.15	0.07	0.32	0.25	0.32	0.32	0.37	0.39	0.33	0.27	0.31	0.29	0.26	0.33
Annual	Day	*0.57*	0.02	0.34	0.31	0.33	0.36	0.42	0.22	0.34	0.05	0.40	0.42	0.31	0.32	0.29	0.37	0.05	0.34	*0.57*	0.29	0.43	0.41
	Night	*0.56*	0.04	0.15	0.17	0.38	0.30	0.22	0.27	0.18	0.00	0.25	0.26	0.28	0.28	0.40	0.16	0.11	0.24	*0.53*	0.22	0.34	0.28

Region: **Ca Sd:** Canadian Shield; Subregion: **1.** Alpine; **2.** Alpine; **3:** Montane; **4:** Upper Foothills; **5:** Lower Foothills; **6:** Dry Mixedgrass; **7:** Mixedgrass; **8:** Northern Fescue; **9:** Foothills Fescue; **10:** Foothills Parkland; **11:** Central Parkland; **12:** Peace River Parkland; **13:** Dry Mixedwood; **14:** Central Mixedwood; **15:** Upper Boreal Highlands; **17:** Athabasca Plain; **18:** Peace–Athabasca Delta; **19:** Northern Mixedwood; **20:** Boreal Subarctic; **21:** Kazan Upland.

Table 6. Relations between day and nighttime LST and AO indices at both monthly and annual timescales, where acceptable correlations ($r \geq 0.50$) are highlighted italic.

Month	Natural Region	Rocky Mountain			Foothills			Grassland			Parkland						Boreal Forest						Ca Sd	Alberta
	Subregion	1	2	3	4	5	6	7	8	9	10	11	12	13	14	15	16	17	18	19	20	21		
Jan	Day	−0.31	−0.29	0.00	−0.25	−0.20	0.17	0.24	0.09	0.26	0.10	−0.09	−0.17	−0.12	0.08	0.05	0.08	0.21	0.23	0.05	0.12	0.08	0.00
	Night	−0.34	−0.37	−0.09	−0.18	−0.12	0.01	0.00	−0.12	−0.05	−0.14	−0.22	−0.14	−0.13	0.02	0.05	0.05	0.10	0.14	0.05	0.07	0.03	−0.06
Feb	Day	−0.41	−0.40	−0.28	−0.30	−0.27	−0.06	−0.11	−0.11	−0.11	−0.20	−0.15	−0.08	−0.21	−0.29	−0.29	−0.30	−0.35	−0.35	−0.39	−0.38	−0.30	−0.26
	Night	−0.43	−0.41	−0.14	−0.27	−0.23	−0.03	−0.08	−0.16	−0.10	−0.15	−0.17	−0.20	−0.26	−0.26	−0.30	−0.28	−0.26	−0.29	−0.40	−0.38	−0.27	−0.25
Mar	Day	−0.21	−0.20	−0.25	−0.20	−0.23	−0.01	−0.08	0.03	−0.10	−0.18	−0.10	−0.21	−0.23	−0.24	−0.21	−0.24	−0.30	−0.24	−0.19	−0.19	−0.27	−0.19
	Night	−0.22	−0.22	−0.14	−0.23	−0.19	−0.10	−0.11	−0.04	−0.09	−0.14	−0.08	−0.21	−0.20	−0.21	−0.23	−0.24	−0.30	−0.22	−0.19	−0.14	−0.29	−0.19
Apr	Day	*−0.58*	*−0.60*	*−0.74*	*−0.56*	*−0.53*	*−0.56*	*−0.61*	*−0.51*	*−0.59*	*−0.74*	*−0.52*	−0.40	−0.44	−0.40	−0.40	−0.40	−0.23	−0.20	−0.33	−0.39	−0.24	*−0.51*
	Night	−0.60	−0.63	−0.64	−0.56	−0.49	−0.45	−0.51	−0.40	−0.53	−0.60	−0.43	−0.36	−0.31	−0.30	−0.34	−0.33	−0.12	−0.08	−0.24	−0.12	−0.16	−0.40
May	Day	0.02	0.02	0.28	0.06	0.09	0.34	0.31	0.21	0.22	0.32	0.23	0.10	0.16	0.10	−0.06	−0.01	0.08	0.09	−0.06	−0.14	0.07	0.12
	Night	0.08	0.11	0.23	0.07	0.05	0.32	0.29	0.22	0.26	0.19	0.10	−0.13	−0.05	0.05	−0.06	−0.02	0.03	0.06	−0.08	−0.07	−0.05	0.06
Jun	Day	*0.50*	*0.51*	0.28	*0.50*	0.47	0.12	0.13	0.09	0.16	0.23	0.15	0.11	0.31	*0.69*	*0.67*	*0.73*	0.48	*0.52*	0.43	*0.51*	*0.51*	0.45
	Night	0.43	0.49	*0.55*	*0.56*	*0.61*	*0.64*	*0.65*	*0.63*	*0.64*	*0.58*	*0.56*	*0.52*	*0.68*	*0.73*	*0.74*	*0.73*	*0.55*	0.37	*0.54*	*0.60*	0.44	*0.77*
Jul	Day	0.14	0.18	0.41	0.18	0.19	0.15	0.28	0.11	0.37	0.47	0.17	0.13	0.18	0.26	0.27	0.30	0.30	0.17	0.19	0.17	0.32	0.26
	Night	0.22	0.23	0.33	0.23	0.27	0.48	0.40	0.38	0.29	0.30	0.30	0.34	0.30	0.35	0.35	0.33	0.41	0.26	0.37	0.37	0.41	0.37
Aug	Day	0.43	0.44	0.28	0.43	0.32	0.21	0.26	0.32	0.36	0.36	0.36	0.13	0.30	0.34	0.43	0.43	0.28	0.27	0.30	0.36	0.24	0.40
	Night	0.24	0.28	0.10	0.40	0.43	0.00	−0.02	0.09	0.10	0.20	0.24	*0.50*	0.45	0.37	0.45	0.28	0.30	0.33	0.49	*0.51*	0.29	0.38
Sep	Day	−0.02	−0.01	−0.04	0.05	0.02	0.00	0.00	−0.06	0.01	−0.05	−0.05	−0.05	−0.02	−0.03	0.18	−0.01	−0.11	−0.10	−0.02	−0.02	−0.05	−0.02
	Night	0.02	0.04	0.03	0.07	0.07	−0.09	−0.02	−0.04	−0.02	0.02	0.00	0.08	0.22	0.05	0.01	0.02	0.02	−0.01	−0.09	−0.04	−0.06	0.02
Oct	Day	0.09	0.11	0.22	0.27	0.30	0.24	0.21	0.19	0.17	0.21	0.18	0.38	0.38	0.42	*0.50*	0.47	0.49	*0.52*	0.45	0.43	0.45	0.36
	Night	0.13	0.14	0.19	0.33	0.40	0.09	0.09	0.17	0.14	0.19	0.31	0.42	0.35	0.48	0.47	0.44	0.48	0.44	0.46	0.38	0.48	0.39
Nov	Day	−0.29	−0.29	−0.15	−0.14	−0.12	−0.11	−0.01	−0.14	−0.08	−0.12	−0.15	−0.04	−0.10	−0.04	−0.09	−0.06	−0.07	−0.09	−0.20	−0.24	−0.09	−0.11
	Night	−0.25	−0.26	−0.16	−0.07	−0.07	−0.16	−0.14	−0.26	−0.19	−0.15	−0.14	−0.07	−0.09	−0.06	−0.08	−0.07	−0.06	−0.12	−0.22	−0.19	−0.09	−0.12
Dec	Day	−0.19	−0.17	−0.01	0.15	0.16	0.19	0.07	0.17	0.10	0.06	0.16	0.30	0.19	0.10	0.07	0.07	−0.06	−0.07	−0.04	−0.05	−0.12	0.10
	Night	−0.15	−0.08	0.34	0.22	0.38	0.23	0.32	0.25	0.33	0.25	0.27	0.42	0.30	0.09	0.11	0.10	−0.07	−0.11	−0.04	−0.03	−0.18	0.17
Annual	Day	−0.16	−0.23	−0.34	−0.20	−0.16	0.07	−0.27	−0.04	−0.10	−0.30	−0.25	−0.22	0.00	−0.07	−0.08	−0.32	−0.28	−0.29	−0.16	−0.22	−0.14	−0.20
	Night	−0.12	−0.27	−0.23	−0.18	0.02	0.02	−0.17	0.16	0.10	−0.31	−0.23	−0.08	0.14	0.19	−0.10	−0.35	−0.23	−0.04	−0.06	−0.20	−0.08	−0.14

Region: **Ca Sd:** Canadian Shield; Subregion: **1.** Alpine; **2.** Alpine; **3:** Montane; **4:** Upper Foothills; **5:** Lower Foothills; **6:** Dry Mixedgrass; **7:** Mixedgrass; **8:** Northern Fescue; **9:** Foothills Fescue; **10:** Foothills Parkland; **11:** Central Parkland; **12:** Peace River Parkland; **13:** Dry Mixedwood; **14:** Central Mixedwood; **15:** Upper Boreal Highlands; **17:** Athabasca Plain; **18:** Peace–Athabasca Delta; **19:** Northern Mixedwood; **20:** Boreal Subarctic; **21:** Kazan Upland.

Table 7. Relations between day and nighttime LST and SST (Niño 3.4) indices at both monthly and annual timescales, where acceptable correlations ($r \geq 0.50$) are highlighted italic.

Month	Natural Region	Rocky Mountain			Foothills			Grassland			Parkland							Boreal Forest					Ca Sd	Alberta
	Subregion	1	2	3	4	5	6	7	8	9	10	11	12	13	14	15	16	17	18	19	20	21	
Jan	Day	0.22	0.19	0.03	−0.04	−0.22	−0.18	−0.19	−0.22	−0.17	−0.04	−0.24	−0.29	−0.20	−0.08	−0.06	−0.01	0.05	0.07	0.05	0.09	0.07	−0.11
	Night	0.38	0.31	0.06	−0.06	−0.10	−0.05	0.00	−0.09	−0.02	0.03	−0.14	−0.16	−0.08	0.07	0.06	0.09	0.13	0.11	0.11	0.12	0.19	0.02
Feb	Day	0.34	0.32	0.30	0.28	0.25	0.26	0.28	0.17	0.25	0.27	0.16	0.15	0.21	0.18	0.19	0.25	0.05	0.07	0.00	0.10	0.00	0.22
	Night	0.36	0.33	0.25	0.30	0.29	0.25	0.28	0.23	0.23	0.23	0.24	0.34	0.27	0.25	0.30	0.29	0.12	0.16	0.17	0.23	0.15	0.28
Mar	Day	0.28	0.32	0.34	0.31	0.30	0.35	0.32	0.35	0.34	0.33	0.35	0.26	0.32	0.31	0.37	0.35	0.25	0.32	0.38	0.36	0.34	0.36
	Night	0.24	0.26	0.20	0.25	0.24	0.23	0.19	0.31	0.20	0.19	0.30	0.24	0.29	0.35	0.36	0.36	0.31	0.39	0.42	0.46	0.37	0.33
Apr	Day	*0.60*	*0.59*	*0.54*	*0.52*	0.47	0.39	0.46	0.32	0.26	*0.57*	0.41	0.46	0.46	0.40	0.40	0.37	0.28	0.25	0.37	0.38	0.25	0.46
	Night	*0.54*	*0.56*	0.43	0.47	0.45	0.35	0.41	0.37	0.44	0.40	0.40	0.29	0.29	0.26	0.31	0.32	0.16	0.19	0.21	−0.01	0.20	0.36
May	Day	0.33	0.28	−0.04	0.19	0.22	0.30	0.17	0.32	0.08	−0.17	0.28	0.34	0.26	0.08	0.21	0.07	0.09	0.07	0.10	0.03	0.05	0.21
	Night	0.12	0.11	−0.13	0.07	−0.02	−0.30	−0.20	−0.32	−0.18	−0.15	−0.29	0.04	−0.06	−0.21	−0.07	−0.07	−0.22	−0.11	−0.14	−0.08	−0.19	−0.15
Jun	Day	0.34	0.31	0.32	0.38	0.40	*0.59*	*0.51*	*0.54*	0.45	0.36	0.48	0.31	*0.53*	0.44	0.49	0.36	0.25	0.26	0.30	0.26	−0.01	*0.57*
	Night	0.46	0.46	0.38	0.37	0.30	0.19	0.28	0.02	0.29	0.34	0.07	0.37	0.27	0.19	0.19	0.19	−0.14	−0.17	−0.12	−0.09	−0.14	0.24
Jul	Day	0.19	0.18	0.21	0.22	0.30	0.44	0.33	*0.52*	0.26	0.34	0.46	0.15	0.44	0.24	0.24	0.09	−0.12	0.15	0.17	0.23	0.00	0.40
	Night	0.28	0.26	0.19	0.18	0.08	0.02	0.08	−0.06	0.09	0.21	−0.05	−0.06	−0.05	−0.04	−0.10	−0.08	−0.18	−0.28	−0.12	−0.18	−0.34	0.01
Aug	Day	0.20	0.15	0.06	0.18	0.33	0.12	0.14	0.24	0.12	0.11	0.41	0.25	0.39	0.24	0.15	0.06	0.03	0.11	0.11	0.09	0.09	0.26
	Night	0.21	0.19	−0.02	0.13	0.02	−0.22	−0.16	−0.11	−0.07	0.03	−0.09	−0.18	−0.12	−0.04	−0.07	−0.05	−0.03	−0.06	−0.09	−0.13	−0.02	−0.05
Sep	Day	−0.02	−0.01	0.05	0.01	0.00	0.03	0.07	0.06	0.08	0.08	0.12	0.10	0.10	0.03	0.15	0.07	0.15	0.19	0.16	0.07	0.18	0.07
	Night	−0.01	0.01	0.06	−0.04	−0.03	0.08	0.05	0.16	0.00	−0.06	0.05	−0.02	0.08	0.01	0.04	0.06	0.07	0.03	0.00	−0.04	0.11	0.02
Oct	Day	0.03	0.03	−0.05	0.02	−0.01	−0.09	−0.06	−0.06	−0.02	−0.04	0.01	0.04	−0.01	0.00	0.01	0.05	0.01	0.02	0.00	0.00	−0.06	−0.01
	Night	0.05	0.04	−0.22	0.02	−0.02	−0.15	−0.23	−0.16	−0.22	−0.26	−0.23	0.00	−0.07	−0.12	−0.05	0.00	−0.08	−0.08	−0.09	−0.03	−0.12	−0.10
Nov	Day	0.14	0.11	−0.17	0.03	−0.02	−0.15	−0.21	−0.04	−0.13	−0.15	0.00	0.00	−0.01	0.05	0.02	0.07	0.02	0.02	0.04	0.06	−0.01	0.00
	Night	0.03	0.04	0.02	0.04	0.05	0.02	0.00	0.18	0.05	0.09	0.11	0.14	0.04	0.06	0.07	0.06	0.03	0.00	−0.01	0.04	−0.01	0.06
Dec	Day	0.08	0.09	0.05	0.18	0.10	0.20	0.14	0.10	0.08	0.06	0.07	0.15	0.09	0.13	0.15	0.23	0.10	0.07	0.14	0.16	0.01	0.13
	Night	0.14	0.15	0.05	0.22	0.22	0.12	0.06	0.20	0.09	0.05	0.15	0.16	0.17	0.20	0.20	0.24	0.25	0.21	0.15	0.12	0.19	0.19
Annual	Day	0.46	0.00	0.19	0.23	0.42	0.34	0.38	0.16	0.29	−0.02	0.32	0.29	0.29	0.21	0.39	0.23	0.06	0.31	0.43	0.19	0.30	0.36
	Night	0.43	−0.03	−0.01	0.04	0.15	0.19	0.12	0.11	0.00	−0.04	0.09	0.12	0.14	0.11	0.22	0.00	−0.04	0.09	0.40	0.08	0.19	0.12

Region: **Ca Sd:** Canadian Shield; Subregion: **1.** Alpine; **2.** Alpine; **3:** Montane; **4:** Upper Foothills; **5:** Lower Foothills; **6:** Dry Mixedgrass; **7:** Mixedgrass; **8:** Northern Fescue; **9:** Foothills Fescue; **10:** Foothills Parkland; **11:** Central Parkland; **12:** Peace River Parkland; **13:** Dry Mixedwood; **14:** Central Mixedwood; **15:** Upper Boreal Highlands; **17:** Athabasca Plain; **18:** Peace–Athabasca Delta; **19:** Northern Mixedwood; **20:** Boreal Subarctic; **21:** Kazan Upland.

5. Discussion

LST is a major element in weather, climate, and natural (ecological) environment research. In this study, we used monthly day and nighttime LST in finding local warming and cooling trends in the natural regions and subregions of Alberta. Results reveal that both warming and cooling trends occurred in the study area. The warming trends were observed in the northern and western regions and subregions (see Figure 3a–d,g–i), and the cooling trends in the south and southeast (see Figure 3c–f,j). The extent and magnitude of the warming trends were more pronounced than cooling. A similar warming trend in the northern part of Alberta was also reported in another study [8]. This warming was mostly in the subregions of the Rocky Mountain and Boreal Forest regions (see Figure 3a,g). The Rocky Mountains are characterized by glaciers, scattered vegetation, non-vegetated steep sloping bedrocks, and receiving the highest amount of snowfall [41]. Warming in such cold Rocky Mountains with high elevations (the highest peak is Mount Robson in Canadian Rockies with 3954 m above mean sea level [53]) in comparison to other land cover at the same latitude would probably be due to the global climate change [54–56]. This region is more sensitive to climate change (particularly increasing global annual mean temperature [2]), where the warming rates are nearly double compared to the global average [3,4]. Such warming possibly accelerates the mechanism of heating surface related to elevation-dependent warming by decreasing snow/ice albedo, changing water vapour and releasing latent heat, and changing surface water vapour and radiative flux [28,30,54,57]. In addition, global warming is likely responsible for observing the warming trends in the Boreal Forest region in this study. It is impacting the ecosystem variables, such as the early onset of spring due to warming [58,59] leading to the onset of early runoff in March and April [60,61] that changes vegetation phenology of the region by wetting the soils early [62]. Wet soils retain more heat than dry soil, and the mechanism of heating land surface requires some additional time (time lag) [63,64]. This is probably the reason why results show the pronounced warming in May (for both day and nighttime) after the onset of runoff in March and April.

In contrast, the cooling trends we observed in the south during July and August (see Figure 3c,d) would probably be due to the increasing and intensified irrigation in the agricultural area during the growing season in the subregions of prairies of Southern Alberta [65] and an increment of July precipitation [66]. In fact, the irrigation area increased by 13.4% in the province during 2000–2019 [65]; that might be the reason for the declining LST trend we found in the agriculture-dominant area in the south and southeastern Alberta. Irrigation and increased precipitation help wetting and moistening soils to increase the latent heat flux between the irrigated agricultural land and atmosphere to decrease the surface temperature [67,68]. While the moist and wet soils cool the surface by evaporation (from soils) and evapotranspiration (from vegetation) mechanisms using the solar radiation during the longer daytime, it retains surface heat when the mechanism ceased during shorter nighttime. This is a probable cause of having warming trends (with low magnitude) at summer nighttime (see Figure 3h,i). In addition, we observed significant cooling trends in the month of November (see Figure 3e,j) that coincided with other studies reported for the same area for the latter half of the last century [69,70]. Such cooling trends could be associated with the decrease in winter precipitation (including November) in Alberta [71], where less precipitation would potentially cause cooler winter temperatures in some places in Canada [72]. Overall, we found declining LST in the late spring and winter (especially October, November, and February) in most of the subregions; however, those were not significant (see Tables 1 and 2). The decreasing and increasing trends of LST (in most cases not significant) over the months in a year neutralized the significant trends in annual LST for both day and nighttime, except daytime declining trends observed in three subregions of Grassland, two of Parkland, and one of Rocky Mountain regions (see Table 1).

In addition, large-scale atmospheric circulations (i.e., teleconnections patterns) might have significant influence in causing local warming [9,33]. Correlation analysis between

monthly LST and teleconnections patterns (i.e., PNA, PDO, AO, and SST Niño 3.4) for the period 2001–2020 showed that the PNA pattern had the most influence in the regions and subregions while moderate from PDO and AO and very little from SST (Niño 3.4). However, we did not find significant correlations of these teleconnections with the months that showed warming and cooling trends during the period 2001–2020. The most pronounced warming trend in the northern and western subregions was observed in May, where the PNA pattern showed the most influence during October to December and February to April. This is obvious because the PNA pattern is one of the most prominent teleconnections with low-frequency variability in the extra-tropical Northern Hemisphere that appears in fall through early spring in Western Canada [32,33]. Moreover, the positive polarity of the PNA pattern in the Canadian prairies is supposed to cause warmer temperatures in winter [73], and therefore, warmer associated land surface; however, we observed a decreasing LST trend in November. In contrast, the least influence we observed was the SST Niño 3.4 because of its concentration between latitudes 5°N-5°S and longitudes 120-170°W [74], where Alberta is between latitudes 49 and 60°N and longitudes 110 and 120°W. In addition, we did not find any significant relationships of LST trends with PDO due to its potential association with SST [75]. Moreover, AO has more influence in the central and eastern parts of Canada during winter [76], and therefore, we did not find significant influence from it as the study area is located in Western Canada.

6. Conclusions

We demonstrated, in this study, the use of MODIS-derived monthly LST in mapping local warming and cooling trends in the 21 natural subregions of Alberta during 2001–2020 and its relationship with large-scale atmospheric circulations. For deriving the spatial extent and magnitude of the local warming and cooling trends in the study area, we applied the Mann–Kendall test and Sen's slope estimator. In addition, in finding the relationships of the warming trend with the atmospheric circulations, we correlated the LST anomaly of each subregion with the anomalies of PNA, PDO, AO, and Niño 3.4 SST teleconnection patterns (i.e., atmospheric oscillations). We found significant warming trends in most of the subregions of the Rocky Mountain and Boreal Forest regions in May during both day and nighttime. A significant cooling trend was observed during the daytime of July and August in the south and southeastern subregions of the Grassland and Parkland regions. In November, we also noticed a significant cooling trend. However, we did not find a significant warming trend in the annual LST, except a daytime declining trend in six subregions. In addition, analysis revealed that the PNA pattern (among the atmospheric oscillations used in this study) had the most influence in the subregions during February to April and October to December. However, none of the atmospheric oscillations showed any significant relationships with the monthly warming trend during 2001–2020. Since the influence of atmospheric oscillations is prevailing and appreciating for a longer period, a longer timescale of LST would be critical in building their relationships. Consequently, we would like to suggest further study using remote-sensing sensors that could provide LST for a longer period, e.g., NOAA satellites and passive microwaves. The outcomes of this study would be useful for policymakers and stakeholders at the local level to develop warming adaptation and mitigation strategies suitable for a sustainable environment. Researchers can also use this study to understand the changing pattern of monthly warming in the context of climate change.

Author Contributions: All authors contributed to the design and implementation of the research and writing of the manuscript under the supervision of Q.K.H. All authors have read and agreed to the published version of the manuscript.

Funding: We received partial funding from: (i) NSERC DG to Q. Hassan and (ii) Tertiary Education Trust Fund (TETFUND) of Nigeria to I. Ejiagha.

Acknowledgments: We would like to thank NASA and NOAA for providing MODIS LST and anomalies of the teleconnections data, respectively, free of charge. We also acknowledge the Government of Alberta for the spatial data of natural regions and subregions of Alberta.

Conflicts of Interest: The authors declare no conflict of interest.

References

1. Jones, P.D.; Lister, D.H.; Osborn, T.J.; Harpham, C.; Salmon, M.; Morice, C.P. Hemispheric and large-scale land-surface air temperature variations: An extensive revision and an update to 2010. *J. Geophys. Res. Atmos.* **2012**, *117*. [CrossRef]
2. Ji, F.; Wu, Z.; Huang, J.; Chassignet, E.P. Evolution of Land Surface Air Temperature Trend. *Nat. Clim. Chang.* **2014**, *4*, 462–466. [CrossRef]
3. Routson, C.C.; Nicholas, P.; Kaufman, D.S.; Michael, P.; Goosse, H.; Shuman, B.N.; Rodysill, J.R.; Ault, T. Mid-latitude net precipitation decreased with Arctic warming during the Holocene. *Nature* **2019**, *568*, 83–87. [CrossRef] [PubMed]
4. Serreze, M.C.; Barry, R.G. Processes and impacts of Arctic amplification: A research synthesis. *Glob. Planet. Chang.* **2011**, *77*, 85–96. [CrossRef]
5. Bush, E.; Lemmen, D.S. (Eds.) *Canada's Changing Climate Report*; Government of Canada: Ottawa, ON, Canada, 2019.
6. IPCC 2013. *Climate Change 2013: The Physical Science Basis. Working Group I Contribution to the Fifth Assessment Report of the Intergovernmental Panel on Climate Change*; Stocker, T.F., Qin, D., Plattner, G.K., Tignor, M.M.B., Allen, S.K., Boschung, J., Nauels, A., Xia, Y., Bex, V., Midgley, P.M., Eds.; Cambridge University Press: Cambridge, UK; New York, NY, USA, 2013; Volume 9781107057, ISBN 9781107415324.
7. McCarthy, M.P.; Best, M.J.; Betts, R.A. Climate change in cities due to global warming and urban effects. *Geophys. Res. Lett.* **2010**, *37*. [CrossRef]
8. Rahaman, K.R.; Hassan, Q.K.; Chowdhury, E.H. Quantification of Local Warming Trend: A Remote Sensing-Based Approach. *PLoS ONE* **2017**, *12*, e0196882. [CrossRef]
9. Yan, Y.; Mao, K.; Shi, J.; Piao, S.; Shen, X.; Dozier, J.; Liu, Y.; Ren, H.-l.; Bao, Q. Driving forces of land surface temperature anomalous changes in North America in 2002–2018. *Sci. Rep.* **2020**, *10*, 6931. [CrossRef]
10. Lynch, M.; Evans, A. *2017 Wildfire Season: An Overview, Southwestern U.S. Special Report*; Ecological Restoration Institute and Southwest Fire Science Consortium, Northern Arizona University: Flagstaff, AZ, USA, 2018.
11. Menne, M.J.; Williams, C.N.; Palecki, M.A. On the reliability of the U.S. surface temperature record. *J. Geophys. Res.* **2010**, *115*. [CrossRef]
12. Mahlstein, I.; Hegerl, G.; Solomon, S. Emerging local warming signals in observational data. *Geophys. Res. Lett.* **2012**, *39*. [CrossRef]
13. Maduako, I.N.; Ebinne, E.; Idorenyin, U.; Ndukwu, R.I. Accuracy Assessment and Comparative Analysis of IDW, Spline and Kriging in Spatial Interpolation of Landform (Topography): An Experimental Study. *J. Geogr. Inf. Syst.* **2017**, *9*, 354–371. [CrossRef]
14. Bhunia, G.S.; Shit, P.K.; Maiti, R. Comparison of GIS-based interpolation methods for spatial distribution of soil organic carbon (SOC). *J. Saudi Soc. Agric. Sci.* **2018**, *17*, 114–126. [CrossRef]
15. Ahmed, M.R.; Hassan, Q.K.; Abdollahi, M.; Gupta, A. Introducing a new remote sensing-based model for forecasting forest fire danger conditions at a four-day scale. *Remote Sens.* **2019**, *11*, 2101. [CrossRef]
16. Akbar, T.A.; Hassan, Q.K.; Ishaq, S.; Batool, M.; Butt, H.J.; Jabbar, H. Investigative Spatial Distribution and Modelling of Existing and Future Urban Land Changes and Its Impact on Urbanization and Economy. *Remote Sens.* **2019**, *11*, 105. [CrossRef]
17. Luintel, N.; Ma, W.; Ma, Y.; Wang, B.; Subba, S. Spatial and temporal variation of daytime and nighttime MODIS land surface temperature across Nepal. *Atmos. Ocean. Sci. Lett.* **2019**, *12*, 305–312. [CrossRef]
18. Olivares-Contreras, V.A.; Mattar, C.; Gutiérrez, A.G.; Jiménez, J.C. Warming trends in Patagonian subantartic forest. *Int. J. Appl. Earth Obs. Geoinf.* **2019**, *76*, 51–65. [CrossRef]
19. Jiménez-Muñoz, J.C.; Sobrino, J.A.; Mattar, C.; Malhi, Y. Spatial and temporal patterns of the recent warming of the Amazon forest. *J. Geophys. Res. Atmos.* **2013**, *118*, 5204–5215. [CrossRef]
20. Aguilar-Lome, J.; Espinoza-Villar, R.; Espinoza, J.C.; Rojas-Acuña, J.; Willems, B.L.; Leyva-Molina, W.M. Elevation-dependent warming of land surface temperatures in the Andes assessed using MODIS LST time series (2000–2017). *Int. J. Appl. Earth Obs. Geoinf.* **2019**, *77*, 119–128. [CrossRef]
21. Qie, Y.; Wang, N.; Wu, Y.; Chen, A. Variations in winter surface temperature of the Purog Kangri Ice Field, Qinghai-Tibetan Plateau, 2001-2018, using MODIS data. *Remote Sens.* **2020**, *12*, 1133. [CrossRef]
22. Fallah Ghalhari, G.; Khoshhal Dastjerdi, J.; Habibi Nokhandan, M. Using Mann Kendal and t-test methods in identifying trends of climatic elements: A case study of northern parts of Iran. *Manag. Sci. Lett.* **2012**, *2*, 911–920. [CrossRef]
23. Gocic, M.; Trajkovic, S. Analysis of changes in meteorological variables using Mann-Kendall and Sen's slope estimator statistical tests in Serbia. *Glob. Planet. Chang.* **2013**, *100*, 172–182. [CrossRef]
24. Rahman, A.-U.; Dawood, M. Spatio-statistical analysis of temperature fluctuation using Mann–Kendall and Sen's slope approach. *Clim. Dyn.* **2017**, *48*, 783–797. [CrossRef]
25. Li, Y.; Wang, L.; Zhang, L.; Wang, Q. Monitoring the Interannual Spatiotemporal Changes in the Land Surface Thermal Environment in Both Urban and Rural Regions from 2003 to 2013 in China Based on Remote Sensing. *Adv. Meteorol.* **2019**, *2019*, 1–17. [CrossRef]

26. Muster, S.; Langer, M.; Abnizova, A.; Young, K.L.; Boike, J. Spatio-temporal sensitivity of MODIS land surface temperature anomalies indicates high potential for large-scale land cover change detection in Arctic permafrost landscapes. *Remote Sens. Environ.* **2015**, *168*, 1–12. [CrossRef]
27. Ejiagha, I.R.; Ahmed, M.R.; Hassan, Q.K.; Dewan, A.; Gupta, A.; Rangelova, E. Use of Remote Sensing in Comprehending the Influence of Urban Landscape's Composition and Configuration on Land Surface Temperature at Neighbourhood Scale. *Remote Sens.* **2020**, *12*, 2508. [CrossRef]
28. Pepin, N.; Deng, H.; Zhang, H.; Zhang, F.; Kang, S.; Yao, T. An Examination of Temperature Trends at High Elevations Across the Tibetan Plateau: The Use of MODIS LST to Understand Patterns of Elevation-Dependent Warming. *J. Geophys. Res. Atmos.* **2019**, *124*, 5738–5756. [CrossRef]
29. Harris, P.P.; Huntingford, C.; Cox, P.M. Amazon Basin climate under global warming: The role of the sea surface temperature. *Philos. Trans. R. Soc. B Biol. Sci.* **2008**, *363*, 1753–1759. [CrossRef]
30. Pepin, N.; Bradley, R.S.; Diaz, H.F.; Baraer, M.; Caceres, E.B.; Forsythe, N.; Fowler, H.; Greenwood, G.; Hashmi, M.Z.; Liu, X.D.; et al. Elevation-dependent warming in mountain regions of the world. *Nat. Clim. Chang.* **2015**, *5*, 424–430. [CrossRef]
31. Hall, D.K.; Williams, R.S.; Luthcke, S.B.; Digirolamo, N.E. Greenland ice sheet surface temperature, melt and mass loss: 2000–2006. *J. Glaciol.* **2008**, *54*, 81–93. [CrossRef]
32. Shabbar, A.; Khandekar, M. The impact of el Nino-Southern oscillation on the temperature field over Canada: Research note. *Atmos.-Ocean* **1996**, *34*, 401–416. [CrossRef]
33. Bonsal, B.; Shabbar, A. *Large-Scale Climate Oscillations Influencing Canada, 1900-2008*; Canadian Biodiversity: Ecosystem Status and Trends 2010. Technical Thematic Report No. 4; Canadian Councils of Resource Ministers: Ottawa, ON, USA,, 2011; 20p.
34. Slonosky, V.C.; Jones, P.D.; Davies, T.D. Impacts of low frequency variability modes on Canadian winter temperature. *Int. J. Climatol.* **2001**, *21*, 95–108. [CrossRef]
35. Chen, Z.; Gan, B.; Wu, L.; Jia, F. Pacific-North American teleconnection and North Pacific Oscillation: Historical simulation and future projection in CMIP5 models. *Clim. Dyn.* **2018**, *50*, 4379–4403. [CrossRef]
36. Rafferty, J.P. North Atlantic Oscillation (Climatology). Available online: https://www.britannica.com/science/North-Atlantic-Oscillation (accessed on 22 June 2021).
37. Statistics Canada. 2001 Census: Alberta Population. Available online: https://www12.statcan.gc.ca/English/profil01/CP01/Details/Page.cfm?Lang=E&Geo1=CMA&Code1=835__&Geo2=PR&Code2=48&Data=Count&SearchText=Edmonton&SearchType=Begins&SearchPR=01&B1=Population&Custom= (accessed on 14 June 2021).
38. Statistics Canada. Census Profile, 2016 Census: Alberta. Available online: https://www12.statcan.gc.ca/census-recensement/2016/dp-pd/prof/details/page.cfm?Lang=E&Geo1=PR&Code1=48&Geo2=PR&Code2=01&SearchText=Alberta&SearchType=Begins&SearchPR=01&B1=Population&TABID=1&type=0 (accessed on 14 June 2021).
39. Government of Alberta. Population Statistics: Alberta population Estimates. Available online: https://www.alberta.ca/population-statistics.aspx (accessed on 14 June 2021).
40. Government of Alberta. Alberta Population Estimates-Data Tables. Municipal (Census Subdivision) Population Estimates: 2016–2020 (updated 23 March 2021). Available online: https://open.alberta.ca/dataset/alberta-population-estimates-data-tables (accessed on 14 June 2021).
41. Natural Regions Committee 2006. *Natural Regions and Subregions of Alberta*; Downing, D.J., Pettapiece, W.W., Eds.; Government of Alberta: Edmonton, AL, Canada, 2006.
42. Achuff, P.L. *Natural Regions, Subregions and Natural History Themes of Alberta: A Classification for Protected Areas Management*; Alberta Environmental Protection: Edmonton, AL, Canada, 1994.
43. Marshall, I.B.; Smith, S.C.A.; Selby, C.J. A national framework for monitoring and reporting on environmental sustainability in Canada. *Environ. Monit. Assess.* **1996**, *39*, 25–38. [CrossRef] [PubMed]
44. Mann, H.B. Nonparametric Tests Against Trend. *Econometrica* **1945**, *13*, 15. [CrossRef]
45. Kendall, M.G. Rank Correlation Methods. *J. R. Stat. Soc. Ser. D. Stat.* **1971**, *20*, 74. [CrossRef]
46. Sen, P.K. Estimates of the Regression Coefficient Based on Kendall's Tau. *J. Am. Stat. Assoc.* **1968**, *63*, 1379–1389. [CrossRef]
47. Nunifu, T.; Long, F. *Methods and Procedures for Trend Analysis of Air QUality Data*; Government of Alberta, Ministry of Environment and Parks: Edmonton, AL, Canada, 2019; ISBN 978-1-4601-3637-9.
48. Kocsis, T.; Kovács-Székely, I.; Anda, A. Comparison of parametric and non-parametric time-series analysis methods on a long-term meteorological data set. *Cent. Eur. Geol.* **2017**, *60*, 316–332. [CrossRef]
49. Hirsch, R.M.; Slack, J.R.; Smith, R.A. Techniques of trend analysis for monthly water quality data. *Water Resour. Res.* **1982**, *18*, 107–121. [CrossRef]
50. Wang, Z.; Lu, Z.; Cui, G. Spatiotemporal variation of land surface temperature and vegetation in response to climate change based on NOAA-AVHRR data over China. *Sustainability* **2020**, *12*, 3601. [CrossRef]
51. Gilewski, P.; Nawalany, M. Inter-comparison of Rain-Gauge, Radar, and Satellite (IMERG GPM) precipitation estimates performance for rainfall-runoff modeling in a mountainous catchment in Poland. *Water* **2018**, *10*, 1665. [CrossRef]
52. Rauf, A.U.; Ghumman, A.R. Impact assessment of rainfall-runoffsimulations on the flow duration curve of the Upper Indus river-a comparison of data-driven and hydrologic models. *Water* **2018**, *10*, 876. [CrossRef]
53. Ommanney, C.S.L. Glaciers of the Canadian Rockies. In *Satellite Image Atlas of the Glaciers of the World—North America*; Williams, R.S., Jr., Ferrignod, J.G., Eds.; U.S. Geological Survey: Reston, VA, USA, 2002; pp. J199–J289.

54. Rangwala, I.; Miller, J.R. Climate change in mountains: A review of elevation-dependent warming and its possible causes. *Clim. Chang.* **2012**, *114*, 527–547. [CrossRef]
55. Beniston, M.; Diaz, H.F.; Bradley, R.S. Climatic change at high elevation sites: An overview. *Clim. Chang.* **1997**, *36*, 233–251. [CrossRef]
56. Messerli, B.; Ives, J.D. *Mountains of the World: A Global Priority*; The Parthenon Publishing Group: New York, NY, USA, 1997.
57. Vuille, M.; Franquist, E.; Garreaud, R.; Casimiro, W.S.L.; Cáceres, B. Impact of the global warming hiatus on Andean temperature. *J. Geophys. Res. Atmos.* **2015**, *120*, 3745–3757. [CrossRef]
58. Bonsal, B.R.; Prowse, T.D. Trends and variability in spring and autumn 0°C-isotherm dates over Canada. *Clim. Chang.* **2003**, *57*, 341–358. [CrossRef]
59. Schwartz, M.D.; Ahas, R.; Aasa, A. Onset of spring starting earlier across the Northern Hemisphere. *Glob. Chang. Biol.* **2006**, *12*, 343–351. [CrossRef]
60. Burn, D.H. Climatic influences on streamflow timing in the headwaters of the Mackenzie River Basin. *J. Hydrol.* **2008**, *352*, 225–238. [CrossRef]
61. Stewart, I.T.; Cayan, D.R.; Dettinger, M.D. Changes toward earlier streamflow timing across western North America. *J. Clim.* **2005**, *18*, 1136–1155. [CrossRef]
62. Deng, G.; Zhang, H.; Guo, X.; Shan, Y.; Ying, H.; Rihan, W.; Li, H.; Han, Y. Asymmetric Effects of Daytime and Nighttime Warming on Boreal Forest Spring Phenology. *Remote Sens.* **2019**, *11*, 1651. [CrossRef]
63. Van Der Velde, R.; Su, Z.; Ek, M.; Rodell, M.; Ma, Y. Influence of thermodynamic soil and vegetation parameterizations on the simulation of soil temperature states and surface fluxes by the Noah LSM over a Tibetan plateau site. *Hydrol. Earth Syst. Sci.* **2009**, *13*, 759–777. [CrossRef]
64. Peters-Lidard, C.D.; Blackburn, E.; Liang, X.; Wood, E.F. The effect of soil thermal conductivity parameterization on surface energy fluxes and temperatures. *J. Atmos. Sci.* **1998**, *55*, 1209–1224. [CrossRef]
65. Government of Alberta. *Alberta Agriculture and Forestry. Alberta Irrigation Information 2019*; Lethbridge: Edmonton, AL, Canada, 2020; 34p.
66. Shen, S.S. *An Assessment of the Change in Temperature and Precipitation in Alberta*; Science and Technology Branch, Environmental Sciences Division, Alberta Environment: Edmonton, AL, Canada, 1999.
67. Liu, T.; Yu, L.; Zhang, S. Land Surface Temperature Response to Irrigated Paddy Field Expansion: A Case Study of Semi-arid Western Jilin Province, China. *Sci. Rep.* **2019**, *9*, 5278. [CrossRef]
68. Yang, Q.; Huang, X.; Tang, Q. Irrigation cooling effect on land surface temperature across China based on satellite observations. *Sci. Total Environ.* **2020**, *705*, 135984. [CrossRef] [PubMed]
69. Gan, T.Y. Hydroclimatic trends and possible climatic warming in the Canadian Prairies. *Water Resour. Res.* **1998**, *34*, 3009–3015. [CrossRef]
70. Chaikowsky, C. *Analysis of Alberta Temperature Observations and Estimates by Global Climate Models*; Environmental Sciences Division, Alberta Environment: Edmonton, AL, Canada, 2000.
71. Newton, B.W.; Farjad, B.; Orwin, J.F. Spatial and temporal shifts in historic and future temperature and precipitation patterns related to snow accumulation and melt regimes in Alberta, Canada. *Water* **2021**, *13*, 1013. [CrossRef]
72. Isaac, G.A.; Stuart, R.A. Temperature–Precipitation Relationships for Canadian Stations. *J. Clim.* **1992**, *5*, 822–830. [CrossRef]
73. Liu, Z.; Yoshmura, K.; Bowen, G.J.; Welker, J.M. Pacific-North American teleconnection controls on precipitation isotopes (δ18O) across the Contiguous United States and Adjacent Regions: A GCM-based analysis. *J. Clim.* **2014**, *27*, 1046–1061. [CrossRef]
74. NOAA. National Centers for Environmental Information. Equatorial Pacific Sea Surface Temperatures. Available online: https://www.ncdc.noaa.gov/teleconnections/enso/indicators/sst/ (accessed on 15 July 2021).
75. Mantua, N.J.; Hare, S.R.; Zhang, Y.; Wallace, J.M.; Francis, R.C. A Pacific Interdecadal Climate Oscillation with Impacts on Salmon Production. *Bull. Am. Meteorol. Soc.* **1997**, *78*, 1069–1079. [CrossRef]
76. Wu, A.; Hsieh, W.W.; Shabbar, A.; Boer, G.J.; Zwiers, F.W. The nonlinear association between the Arctic Oscillation and North American winter climate. *Clim. Dyn.* **2006**, *26*, 865–879. [CrossRef]